Ionic liquids for electrochemical applications: Correlation between molecular structure and electrochemical stability window

Ionic liquids for electrochemical applications: correlation between molecular structure and electrochemical stability window

Erik Piatti[a], Luca Guglielmero[b,c,§], Giorgio Tofani[b,d,*], Andrea Mezzetta[b], Lorenzo Guazzelli[b], Felicia D'Andrea[b], Stefano Roddaro[d,e] and Christian Silvio Pomelli[b,*]

[a] *Department of Applied Science and Technology, Politecnico di Torino, Torino, Italy*

[b] *Department of Pharmacy, University of Pisa, Pisa, Italy*

[c] *Scuola Normale Superiore, Classe di Scienze, Pisa, Italy*

[d] *Department of Physics, University of Pisa, Pisa, Italy*

[e] *NEST, CNR—Istituto Nanoscienze and Scuola Normale Superiore, Pisa, Italy*

* *Corresponding authors*

[§] *Co-first author*

e-mail corresponding authors: Giorgio Tofani: giorgio.tofani@df.unipi.it

Christian Silvio Pomelli: christian.pomelli@unipi.it

Abstract

Ionic gating has emerged as an effective and versatile tool to tune the charge-carrier density of a material and control its electronic ground state, as well as to develop low-temperature devices such as electrochemical transistors. Ionic liquids are a promising gating agent due to their high thermal- and electrochemical stability for both fundamental and applied research. However, the understanding of the correlation between the molecular structure of ionic liquids and their electrochemical stability is quite limited. For this reason, this study aims at determining the guidelines for synthesizing ionic liquids suitable for their use as electrolytes at low temperatures. A series of twenty-three ionic liquids having various ammonium cations, composed of three "short chains" and one "long chain", and Tf_2N as the anion, were synthesized. Afterwards, their thermal behavior was determined to identify those ionic liquids exhibiting T_g< -50 °C. The anodic and cathodic limits of the selected ionic liquids were measured via linear-sweep voltammetry using an electrochemical transistor configuration, working at -33 °C. Electrochemical windows having absolute values from 2.9 to 5.7 V were measured. Overall, five guidelines were determined from the experimental results: first, the cations influence both cathodic and anodic limits; second, the asymmetric ammonium cations show larger electrochemical stability than symmetric ones; third, the electrochemical stability decreases at the increase of the length of the "long chain"; fourth, alkyl long chains show a larger anodic limit, but smaller cathodic limit than ether long chains having the same length; fifth, the ether chain with largest electrochemical stability comprises three carbon atoms and one oxygen.

Keywords

Ionic gating, Ionic liquids, thermal behavior, thermal stability, electrochemical stability, electrochemical window.

1. Introduction

Tuning the charge-carrier density of a material is one of the most well-established means to control its electronic ground state and affect its physical properties, and it is widely employed from fundamental physics to applied electronics and energy storage. In the last two decades, ionic gating has emerged as an effective and versatile tool for this purpose, owing to the extremely large charge densities induced by the ultra-high electric fields attainable in the electric double layer (EDL) formed at voltage-polarized solid-electrolyte interfaces [1–3]. In the standard ionic-gating setup, the material of choice acts as the active channel of an electrochemical transistor, and its charge-carrier density is controlled via the electric potential applied across the chosen electrolyte by biasing the gate counter-electrode [1–3]. Beyond a simple tuning of the electrical conductivity [4,5], ionic gating has enabled the electrical control over insulator-to-metal [6–11], superconductive [12–20] and magnetic [21–25] phase transitions and shown promise for applications including logic circuits [26–29], memory devices [30,31], chiral-light emitting transistors [32], stretchable/flexible devices [26,33,34], thermoelectric energy harvesters [35]. Early reports chiefly made use of polymeric electrolytes as the gate ionic medium [12], but these were mostly phased out in favor of ionic liquids (ILs) or ion gels, thanks to their large capacitances, low melting points, and wide electrochemical windows [1–3]. The combination of these properties made ILs especially advantageous for ionic gating, as it allowed significantly increasing the maximum applicable gate voltages before the onset of undesired electrochemical reactions in the transistor, thereby extending the range of maximum attainable charge-density modulations [1,9,10,13,16]. The possibility to increase the maximum applied gate voltage was found to be particularly important in systems where the total gate capacitance was upper-bounded not by the geometrical capacitance of the ILs, but either by the necessity to separate a surface-sensitive active material from the ILs by a dielectric encapsulation layer [17,18,36–40] or by the intrinsic low density of states of the gated material (quantum capacitance) [41–44]. Moreover, it has been recently demonstrated that – even in materials with a large density of states – electrostatic correlations between the charged layers in the EDL could give rise to an unexpected “cross” quantum capacitance [45–47], making the issue of reduced gate capacitance in ionic transistors more ubiquitous than previously thought. Consequently, understanding how to design electrolytes with extended electrochemical windows is currently highly desirable from both a fundamental and an applied standpoint.

ILs are salts composed of an organic cation and either organic or inorganic anion that can avoid the formation of organized crystalline structures, keeping the melting point below 100 °C [48,49]. ILs found a wide range of applications [50] for instance as actuators [51,52] and chemical reaction media [53,54] or in the electrochemistry research area, such as gating agents for transistors [9,10], supercapacitors [55], fuel cells [56], and electrolytes for batteries [57,58],. This high interest is related to the possibility of tailoring ILs physico-chemical characteristics for a specific application by changing their molecular structure, giving them the title of "designer solvents" [59]. Furthermore, ILs show valuable physico-chemical properties such as high thermal and chemical stability [60,61] as well as reduced volatility [62,63] and low flammability, [64] which increase their safety when compared with traditional organic solvents. The interest in ILs as electrolytes for various applications has rapidly grown during the last few years. Three main properties determine their success in this field. First, wide electrochemical stability windows allow high voltages during gating uses [1,13] and make ILs valuable electrolytes in high-cell-potentials battery applications [65], while the large ionic conductivity reduces the

charge/discharge time and the internal resistance of electrochemical devices [1]. Second, the good solvent properties displayed by ILs, as well as the tolerability of their solubility characteristics, make this class of compounds very promising both for the solubilization of redox-active compounds and for the realization of innovative redox systems [66,67]. Third, the low melting point displayed by many ILs (often below 0 °C) allows ILs to be used for low-temperature applications such as transistors [9]. Furthermore, the liquid state of IL electrolytes allows the formation of thin layers reducing the mechanical stress, with this property representing a crucial aspect for micrometric devices [13,16]. According to the law of Arrhenius, the kinetic rate of the reactions is suppressed or reduced with the decrease of the temperature [1,9,10,16]. The possibility of working at low temperatures therefore expands the electrochemical stability windows of ILs, since the unwanted electrochemical processes which cause the degradation of the device parts (electrolyte and electrodes) are suppressed or at least reduced. Zhang *et al*. [9] reported that potential chemical reactions between an IL (DEME Tf_2N) and the electrode surface were suppressed when a high voltage was applied under high vacuum and at a temperature just above the glass transition temperature of the IL (i.e., -53 °C). At the same time, the different thermal expansion coefficients between the ILs and the metal electrodes could cause severe mechanical damage to the devices when the experiment is conducted at low temperatures [9]. Consequently, the studies must be performed using highly stable metals.

Several scientific papers studied the electrochemical stability of ILs. However, the different analytical conditions, such as temperature and types of electrodes, do not permit a clear comparison between the studies [68–71]. Despite the consideration that the oxidation of the anions represents the limit for the anodic window, and the reduction of the cation is the main responsible for the cathodic limits, in some publications, it was observed that ILs with the same cations or anions showed different electrochemical stability windows [72]. Zhao *et al*. [73] suggested that the association of anions or cations could play an important role in their electrochemical stabilities. For all these limitations, the comparison between the EW reported in the literature, and the experimental data is not always possible [74].

Nowadays, DEME Tf_2N (**14**) is one of the most used ILs for gating applications due to its low melting temperature, high thermal and electrochemical stability [75]. However, to the best of our knowledge, no reported studies demonstrate its superior performance over other ILs by comparing it with similar ammonium cations. Due to the fragmentation of experimental data and the difficulty to compare the different studies, it is hard to identify clear trends that describe how the structure affects the electrochemical window both from experimental data [76–78] and theoretical studies [79–82]. Nevertheless, some observations can be made. The anodic stability depends on the length of the longest alkyl chain of the ILs based on aliphatic quaternary ammonium salts [77,83]. The shorter this length is, the higher is the oxidation potential. With the same longest chain length, the oxidation stability depends on the other alkyl chain length, showing wider stability when the side alkyl chains are as short as possible [83]. Regarding piperidinium-based ILs, Montanino *et al.* [84] observed that the cathodic limit becomes wider with increasing main alkyl chain length. Instead, the anodic limit is almost stable. Ether functionalities show lower electrochemical stability than alkyl groups having the same length in a more or less visible way [76,77,85,86]. Nokami *et al.* [87] observed that ILs having an ether chain with one oxygen atom showed that the oxygen atom located far from the positively charged nitrogen atom decreased the anodic potential limits.

Due to the high interest in ILs as gating agents for device applications and fundamental research, a more in-depth study is necessary to expand the knowledge on the influence of the ILs' molecular structure on their electrochemical stability. In this study, 23 ammonium cations having three "short chains" and a fourth "long chain" were selected because this structure showed to be the one having better performances from the thermal and electrochemical point of view than other

cations structures [72,74]. The bis(trifluoromethyl sulfonyl)imide anion (Tf_2N) was selected as an anion due to its high conductivity, hydrophobic behavior, wide electrochemical windows, and the possibility of forming liquid ILs at temperatures below 0 °C [76]. Afterwards, the electrochemical stability of the resulting ILs was studied using electrochemical transistors cells to simulate their "real application field" as gating agents in transistors. As reported above, the electrochemical windows increase with the decrease of the operative temperature because the side reactions are reduced. For this reason, it was decided to measure the electrochemical stability at low temperature (-33 °C), trying to obtain the "effective" electrochemical windows where degradation reactions are suppressed or at least reduced.

2. Experimental

2.1 Materials

Trimethylamine (ca. 28% in water, ca. 4.3 mol/L), n-octyl-trimethylammonium bromide (> 98%), 2-bromoethyl ethyl ether (>95%), 1-bromo-2-(2-methoxy ethoxy) ethane (stabilized with Na_2CO_3, >90%), 2-bromoethyl methyl ether (>95%), bromomethyl methyl ether (>95%) were purchased from TCI. 1-methylpyrrolidine (>99%) was purchased from Fluka™. 1-bromobutane (99%), 1-bromopentane (99%), 1-bromohexane (99+%) 1-bromooctane (99%) were purchased from Acros Organics. Triethylamine (>99.5%), *N*-methylpiperidine (99%), *N*,*N*-dimethylethylamine (99%), *N*,*N*-diethylmethylamine (97%), acetonitrile (>99.5%), tetrahydrofuran anhydrous (250 ppm BHT as inhibitor, >99.9%), dichloromethane (>99.5%) and diethyl ether (>99.5%), Deuterated solvents ($CDCl_3$, DMSO-d_6 and CD_3OD) were obtained from Sigma Aldrich (Merck Life Science S.r.l.). Lithium bis(trifluoromethyl sulfonyl)imide ($LiTf_2N$, battery grade) was acquired from IOLITEC. All the employed reagents and solvents were used without further purifications where not differently mentioned.

2.2 General methods

2.2.1 Synthesis of compounds

The synthesis of the ionic liquids studied in this work consisted of two steps. First, the quaternarization of the tertiary amines with aliphatic/ether bromide chains. Second, the anion metathesis reaction with $LiTf_2N$ for the anion exchange.

Quaternarization method A. The procedure was done according to Mezzetta *et al.* [88] with modifications. Two grams of aliphatic/ether bromide chain, tertiary amine in 10 % of molar excess with respect to the aliphatic/ether bromide chain and 15 mL of acetonitrile were added in a flask of 50 mL and stirred for 48 h at a temperature depending on the tertiary amine. 30 °C for the *N*,*N*-dimethylethylamine, 50 °C for the *N*,*N*-diethylmethylamine, 60 °C for the *N*-methylpiperidine and 1-methylpyrrolidine and 70 °C for triethylamine. Diethyl ether was added to the final mixture to precipitate the desired product and eliminate unreacted chemicals. The solid precipitates were filtered under vacuum, washed with diethyl ether, and dried in vacuo to afford white solids products.

Quaternarization method B. The procedure was done according to Mezzetta *et al.* [88] with modifications. Two grams (1.09 mmol) of 1-bromo-2-(2-methoxy ethoxy) ethane, *N*,*N*-diethylmethylamine in 10 % of molar excess with respect to

the ether bromide chain and 15 mL of acetonitrile were added in a flask of 50 mL and stirred for 48 h at 50 °C. The precipitation of a white solid was observed. At the end of the reaction, the liquid phase was removed, and the white solid was washed with diethyl ether to eliminate unreacted chemicals. Next, the solid was filtered under vacuum, washed again with diethyl ether and dried in vacuo to afford white solids products.

Quaternarization method C. According to Zhou *et al.* [89], the procedure was done with modifications. 0.500 g (4 mmol) of bromomethyl methyl ether in 3 mL of anhydrous tetrahydrofuran were added dropwise to a stirred solution of 0.400 g (5.47 mmol) of *N,N*-dimethylethylamine and 7 mL of anhydrous tetrahydrofuran at 0 °C under an argon atmosphere in a flask of 50 mL. The suspension was stirred for 4 h at room temperature. The THF solution was removed, and the solid was washed with diethyl ether and dried under vacuum.

Quaternarization method D. According to Zhou *et al.* [77], the procedure was done with modifications. 20 mL of trimethylamine (ca. 28 % in water, ca. 4.3 mol L^{-1}) and 2.00 g of aliphatic/ether bromide chain were added to a flask of 50 mL and stirred for 96 h at room temperature. The water was removed by drying under vacuum. Afterwards, the resulting product was dissolved in 5 mL of acetonitrile. Diethyl ether was added to precipitate the desired product and eliminate unreacted chemicals. The solid precipitates were filtered under vacuum, washed with diethyl ether, and dried in vacuo to afford white solids products.

The compound n-octyl-trimethylammonium bromide was purchased. All synthesized intermediate compounds have been characterized by NMR spectroscopy.

Anion metathesis procedure. The procedure was done according to Mezzetta *et al.* [88] with modifications. One gram of ammonium bromide compounds from the previous stage was solubilized in 20 mL of water, and lithium bis(trifluoromethyl sulfonyl)imide, in 10% molar excess with respect to the ammonium bromide compounds, was added. The resulting mixture was stirred at room temperature for 2 h and extracted with 20 mL of dichloromethane. The organic phase was washed with water (3 x 7 mL). Afterwards, the dichloromethane was removed under reduced pressure to afford the ionic liquid. The absence of lithium bromide at the end of the purification was checked using silver nitrate added to the final water phase and one drop of the resulting ionic liquid. All synthesized compounds have been characterized by ^{1}H, ^{13}C NMR and FTIR analysis.

1-(2-Methoxyethyl)-1-methyl-piperidinium bis(trifluoromethyl sulfonyl)imide $Pip_{1,2O1}$ (1). The preparation of **1** (78% yield, colorless liquid) was performed according to quaternarization method A followed by metathesis procedure. ^{1}H NMR ($CDCl_3$) δ 3.78-3.76 (m, 2H, OCH_2), 3.54-3.51 (m, 2H, NCH_2CH_2O), 3.47-3.41 (m, 2H, NCH_2 ring), 3.38-3.31(m, 5H, NCH_2 ring, OCH_3), 3.09 (m, 3H, NCH_3), 1.91-1.85 (m, 4H, 2×NCH_2CH_2 ring), 1.76-1.69 (m, 2H, $NCH_2CH_2CH_2$ ring); ^{13}C NMR ($CDCl_3$) δ 121.52 and 118.33 (q, $J_{C,F}$= 319 Hz, 2xCF_3), 65.66 (OCH_2), 62.80 (NCH_2CH_2O), 62.61 (2×NCH_2 ring), 59.08 (OCH_3), 49.25 (NCH_3), 20.62 ($NCH_2CH_2CH_2$ ring), 20.04 (2×$NCH_2CH_2CH_2$ ring); IR (cm^{-1}): 2951.0, 1470.4, 1347.2, 1176.1, 1131.9, 1050.9, 940.4, 876.1, 788.3, 739.5, 653.9 and 612.4. ^{1}H-NMR and ^{13}C-NMR are in accordance with the literature [90].

1-Butyl-1-methyl-piperidinium bis(trifluoromethyl sulfonyl)imide $Pip_{1,4}$ (2). The preparation of **2** (80% yield, colorless liquid) was performed according to quaternarization method A and followed by metathesis procedure. ^{1}H NMR

(DMSO-d_6) δ 3.33-3.26 (m, 6H, 3×NCH_2), 2.98 (m, 3H, NCH_3), 1.78-1.77 (m, 4H, 2×NCH_2CH_2 ring), 1.66-1.62 (m, 2H, $NCH_2CH_2CH_2$ ring), 1.56-1.52 (m, 2H, NCH_2CH_2 chain), 1.35-1.29 (m, 2H, CH_2CH_3), 0.96-0.92 (m, 3H, CH_2CH_3).^{13}C NMR (DMSO-d_6) δ 121.10 and 117.90 (q, $J_{C,F}$= 320 Hz, 2xCF_3), 62.29 (NCH_3), 60.00 (3×NCH_2), 46.97 (NCH_2CH_2 chain), 22.95 ($NCH_2CH_2CH_2$ ring), 20.68 (CH_2CH_3), 19.25 (2×NCH_2CH_2 ring), 13.40 (CH_2CH_3); IR (cm^{-1}): 2966.1, 2880.5, 1467.5, 1347.0, 1175.4, 1133.3, 1051.2, 937.7, 788.4, 739.3, 653.8, 612.5 and 568.7. ^{1}H-NMR, ^{13}C-NMR and FTIR are in accordance with the literature [91].

1-Methyl-1-octyl-piperidinium bis(trifluoromethyl sulfonyl)imide $Pip_{1,8}$ (3). The preparation of **3** (76% yield, colorless liquid) was performed according to quaternarization method A and followed by metathesis procedure. ^{1}H NMR (DMSO-d_6) δ 3.33-3.25 (m, 6H, 3×NCH_2), 2.97 (m, 3H, NCH_3), 1.78-1.76 (m, 4H, 2×NCH_2CH_2 ring), 1.66-1.63 (m, 2H, $NCH_2CH_2CH_2$ ring), 1.56-1.52 (m, 2H, NCH_2CH_2 chain), 1.30-1.27 (m, 10H, $CH_2CH_2CH_2CH_2CH_2CH_2CH_3$), 0.89-0.85 (m, 3H, CH_2CH_3); ^{13}C NMR (DMSO-d_6) δ 121.09 and 117.89 (q, $J_{C,F}$= 320 Hz, 2xCF_3), 62.49 (NCH_3), 59.96 (3×NCH_2), 46.93 (NCH_2CH_2 chain), 31.14 ($NCH_2CH_2CH_2$ chain), 28.44 ($NCH_2CH_2CH_2$ ring), 25.83 ($NCH_2CH_2CH_2CH_2$ chain), 22.01 ($CH_2CH_2CH_2CH_3$), 20.92 ($CH_2CH_2CH_3$), 20.67 (CH_2CH_3), 19.24 (2×NCH_2CH_2 ring), 13.83 (CH_2CH_3); IR (cm^{-1}): 2930.7, 2860.3, 1468.2, 1347.7, 1177.7, 1134.1, 1052.6, 940.8, 883.8, 788.3, 739.3, 653.7, 614.2 and 569.2. ^{1}H-NMR is in accordance with the literature [92].

1-(2-Methoxyethyl)-1-methyl-pyrrolidinium bis(trifluoromethyl sulfonyl)imide $Py_{1,2O1}$ (4). The preparation of **4** (78% yield, colorless liquid) was performed according to quaternarization method A and followed by metathesis procedure. ^{1}H NMR (CD_3OD) δ 3.83-3.80 (m, 2H, OCH_2), 3.60-3.56 (m, 6H, 3×NCH_2), 3.40 (m, 3H, OCH_3), 3.11 (m, 3H, NCH_3), 2.24-2.20 (m, 4H, 2×NCH_2CH_2 ring); ^{13}C NMR (CD_3OD) δ 122.69 and 119.50 (q, $J_{C,F}$= 319 Hz, 2×CF_3), 67.43 (OCH_2), 66.27 (3xNCH_2), 64.39 (OCH_3), 59.04 (NCH_3), 22.25 (2×NCH_2CH_2 ring); IR (cm^{-1}): 2900.1, 1462.9, 1347.5, 1176.0, 1131.2, 1051.0, 996.3, 933.1, 788.7, 739.6, 654.1 and 613.1. ^{1}H-NMR and FTIR are in accordance with the literature [86].

1-Butyl-1-methyl-pyrrolidinium bis(trifluoromethyl sulfonyl)imide $Py_{1,4}$ (5). The preparation of **5** (89% yield, colorless liquid) was performed according to quaternarization method A and followed by metathesis procedure. ^{1}H NMR (DMSO-d_6) δ 3.47-3.40 (m, 4H, 2×NCH_2 ring), 3.35-3.27 (m, 2H, NCH_2 chain), 2.98 (m, 3H, NCH_3), 2.09 (m, 4H, 2×NCH_2CH_2 ring), 1.70-1.66 (m, 2H, $CH_2CH_2CH_3$), 1.35-1.29 (m, 2H, CH_2CH_3), 0.95-0.92 (m, 3H, CH_2CH_3); ^{13}C NMR (DMSO-d_6) δ 122.69 and 119.50 (q, $J_{C,F}$= 319 Hz, 2×CF_3), 63.45 (2×NCH_2 ring), 63.00 (NCH_2 chain), 47.70 (NCH_3), 24.93 ($CH_2CH_2CH_3$), 21.06 (2×NCH_2CH_2 ring), 119.27 (CH_2CH_3), 13.33 (CH_2CH_3); IR (cm^{-1}): 2969.6, 2881.5, 1467.9, 1347.4, 1175.5, 1133.2, 1051.1, 928.1, 788.6, 739.3, 654.0 and 612.8. ^{1}H-NMR, ^{13}C-NMR and FTIR are in accordance with the literature [93].

1-Methyl-1-octyl-pyrrolidinium bis(trifluoromethyl sulfonyl)imide $Py_{1,8}$ (6). The preparation of **6** (79% yield, yellowish liquid) was performed according to quaternarization method A and followed by metathesis procedure. ^{1}H NMR ($CDCl_3$) δ 3.53-3.48 (m, 4H, 2×NCH_2 ring), 3.31-3.27 (m, 2H, NCH_2 chain), 3.04 (m, 3H, NCH_3), 2.28-2.25 (m, 4H, 2×NCH_2CH_2 ring), 1.76-1.72 (m, 2H, NCH_2CH_2 chain), 1.35-1.29 (m, 10H, $CH_2CH_2CH_2CH_2CH_2CH_3$), 0.89-0.86 (m, 3H, CH_2CH_3); ^{13}C NMR ($CDCl_3$) δ 121.53 and 118.34 (q, $J_{C,F}$= 319 Hz, 2×CF_3), 64.97 (NCH_2 chain), 64.70 (2×NCH_2 ring), 48.62 (NCH_3), 31.63 (NCH_2CH_2 chain), 28.99 ($CH_2CH_2CH_2CH_2CH_2CH_3$ chain), 26.25 ($CH_2CH_2CH_2CH_3$), 23.93 ($CH_2CH_2CH_3$), 22.60 (CH_2CH_3), 21.64 (2×NCH_2CH_2 ring), 14.06 (CH_2CH_3); IR (cm^{-1}): 2930.4, 2860.0, 1468.4, 1348.0,

1177.9, 1134.0, 1052.5, 931.2, 788.5, 739.3, 653.7 and 614.2. ^{1}H-NMR, ^{13}C-NMR and FTIR are in accordance with the literature [94].

***N,N,N*-Triethyl-2-methoxy-ethanaminium bis(trifluoromethyl sulfonyl)imide $N_{222,2O1}$ (7).** The preparation of **7** (74% yield, white solid) was performed according to quaternarization method A and followed by metathesis procedure. ^{1}H NMR ($CDCl_3$) δ 3.71-3.70 (m, 2H, OCH_2), 3.41-3.30 (m, 11H, 4×NCH_2, OCH_3), 1.31-1.28 (m, 9H, 3×NCH_2CH_3); ^{13}C NMR ($CDCl_3$) δ 121.55 and 118.35 (q, $J_{C,F}$= 320 Hz, 2×CF_3), 65.63 (OCH_2), 59.22 (OCH_3), 56.78 (NCH_2CH_2O), 54.02 (3×NCH_2CH_3), 7.49 (3xNCH_2CH_3); IR (cm^{-1}): 2997.8, 1472.4, 1397.2, 1347.7, 1176.5, 1132.6, 1051.3, 888.0, 787.1, 739.4, 653.7, 612.7 and 569.5. ^{1}H-NMR is in accordance with the literature [77].

***N,N,N*-Triethyl-1-octanaminium bis(trifluoromethyl sulfonyl)imide $N_{222,8}$ (8).** The preparation of **8** (70% yield, colorless liquid) was performed according to quaternarization method A and followed by metathesis procedure. ^{1}H NMR ($CDCl_3$) δ 3.24-3.19 (m, 6H, 3×NCH_2CH_3), 3.05-3.01 (m, 2H, NCH_2CH_2 chain), 1.60-1.56 (m, 2H, NCH_2CH_2), 1.31-1.23 (m, 19H, 3×NCH_2CH_3, $CH_2CH_2CH_2CH_2CH_2CH_2CH_3$), 0.86-0,82 (m, 3H, CH_2CH_3); ^{13}C NMR ($CDCl_3$) δ 121.52 and 118.32 (q, $J_{C,F}$= 320 Hz, 2×CF_3), 57.23 (NCH_2CH_2), 52.99 (3×NCH_2CH_3), 31.57 (NCH_2CH_2), 28.96 ($NCH_2CH_2CH_2$), 28.90 ($CH_2CH_2CH_2CH_2CH_3$), 26.20 ($CH_2CH_2CH_2CH_3$), 22.53 ($CH_2CH_2CH_3$), 21.62 (CH_2CH_3), 14.00 (CH_2CH_3), 7.27 (3×NCH_2CH_3); IR (cm^{-1}): 2930.1, 2859.7, 1460.5, 1396.8, 1348.2, 1177.4, 1134.7, 1052.6, 788.6, 739.1, 653.5, 614.3 and 569.3. ^{1}H-NMR and ^{13}C-NMR are in accordance with the literature [95].

***N*-Ethyl-2-methoxy-*N,N*-dimethyl-ethanaminium bis(trifluoromethyl sulfonyl)imide $N_{211,2O1}$ (9).** The preparation of **9** (68% yield, colorless liquid) was performed according to quaternarization method A and followed by metathesis procedure. ^{1}H NMR (CD_3OD) δ 3.80-3.77 (m, 2H, OCH_2), 3.53-3.51 (m, 2H, NCH_2CH_2O), 3.49-3.43 (m, 2H, NCH_2CH_3), 3.38 (m, 3H, OCH_3), 3.09 (m, 6H, 2×NCH_3), 1.38-1.34 (m, 3H, NCH_2CH_3); ^{13}C NMR (CD_3OD) δ 122.72 and 119.54 (q, $J_{C,F}$= 318 Hz, 2×CF_3), 66.91 (OCH_2), 63.97-62.15 (NCH_2CH_2O, NCH_2CH_3), 59.08 (OCH_3), 51.52 (2×NCH_3), 8.41 (NCH_2CH_3); IR (cm^{-1}): 2997.8, 2943.4, 2898.1, 1473.4, 1347.2, 1176.5, 1132.9, 1051.3, 960.8, 918.1, 857.5, 789.1, 739.8, 654.3 and 612.5. ^{1}H-NMR and FTIR are in accordance with the literature [96].

***N*-Ethyl-*N,N*-dimethyl-1-butanaminium bis(trifluoromethyl sulfonyl)imide $N_{211,4}$ (10).** The preparation of **10** (65% yield, colorless liquid) was performed according to quaternarization method A and followed by metathesis procedure. ^{1}H NMR (CD_3OD) δ 3.36-3.31 (m, 2H, NCH_2 chain), 3.30-3.25 (m, 2H, NCH_2CH_3), 3.04 (m, 6H, 2×NCH_3), 1.78-1.69 (m, 2H, NCH_2CH_2 chain), 1.46-1.39 (m, 2H, CH_2CH_3), 1.38-1.33 (m, 3H, NCH_2CH_3), 1.04 (m, 3H, $CH_2CH_2CH_3$); ^{13}C NMR (CD_3OD) δ 122.79 and 119.61 (q, $J_{C,F}$= 318 Hz, 2×CF_3), 64.70-60.68 ((NCH_2 chain, NCH_2CH_3), 50.61 (2×NCH_3), 25.38 (NCH_2CH_2 chain), 20.63 (q, 2H, CH_2CH_3), 13.83 ($CH_2CH_2CH_3$), 8.33 (NCH_2CH_3); IR (cm^{-1}): 2970.1, 2882.1, 1470.2, 1347.1, 1176.4, 1133.4, 1051.3, 920.0, 789.0, 739.7, 612.9 and 569.0. ^{1}H-NMR and FTIR are in accordance with the literature [86].

***N*-Ethyl-*N,N*-dimethyl-1-pentanaminium bis(trifluoromethyl sulfonyl)imide $N_{211,5}$ (11).** The preparation of **11** (82% yield, colorless liquid) was performed according to quaternarization method A and followed by metathesis procedure. ^{1}H NMR ($CDCl_3$) δ 3.43-3.38 (m, 2H, NCH_2 chain), 3.25-3.21 (m, 2H, NCH_2CH_3), 3.06 (m, 6H, 2×NCH_3), 1.73-1.69 (m, 2H, NCH_2CH_2 chain), 1.39-1.37 (m, 7H, $CH_2CH_2CH_3$, NCH_2CH_3), 0.95-0.91 (m 3H, $CH_2CH_2CH_3$); ^{13}C NMR ($CDCl_3$) δ 121.50 and 118.31 (q, $J_{C,F}$= 319 Hz, 2×CF_3), 64.25 (NCH_2 chain), 59.99 (NCH_2CH_3), 50.45 (2×NCH_3), 28.11

(NCH_2CH_2 chain), 22.13 ($CH_2CH_2CH_2CH_3$), 13.71 ($CH_2CH_2CH_3$), 8.19 (NCH_2CH_3); IR (cm^{-1}): 2963.6, 2877.4, 1469.2, 1347.3, 1176.9, 1133.8, 1051.7, 788.9, 739.6 and 612.4. ^{1}H-NMR and ^{13}C-NMR are in accordance with the literature [78].

***N*-Ethyl-*N,N*-dimethyl-1-hexanaminium bis(trifluoromethyl sulfonyl)imide $N_{211,6}$ (12).** The preparation of **12** (85% yield, colorless liquid) was performed according to quaternarization method A and followed by metathesis procedure. ^{1}H NMR ($CDCl_3$) δ 3.39-3.34 (m, 2H, NCH_2 chain), 3.22-3.18 (m, 2H, NCH_2CH_3), 3.02 (m, 6H, 2×NCH_3), 1.70-1.64 (m, 2H, NCH_2CH_2 chain), 1.37-1.30 (m, 9H, $CH_2CH_2CH_2CH_3$, NCH_2CH_3), 0.90-0.87 (m, 3H, $CH_2CH_2CH_3$); ^{13}C NMR ($CDCl_3$) δ 121.50 and 118.31 (q, $J_{C,F}$= 319 Hz, 2×CF_3), 64.25 (NCH_2 chain), 59.97 (NCH_2CH_3), 50.37 (2×NCH_3), 31.09 ($NCH_2CH_2CH_2$), 25.72 (NCH_2CH_2) , 22.52 ($CH_2CH_2CH_3$), 22.35 ($CH_2CH_2CH_3$), 13.8 ($CH_2CH_2CH_3$), 8.13 (NCH_2CH_3); IR (cm^{-1}): 2961.0, 2934.6, 2865.6, 1468.9, 1347.4, 1177.2, 1134.0, 1052.1, 788.9, 739.5, 612.8 and 569.4. NMR and FTIR are reported in supporting information (Figure S1 and Figure S6).

***N*-Ethyl-*N,N*-dimethyl-1-octanaminium bis(trifluoromethyl sulfonyl)imide $N_{211,8}$ (13).** The preparation of **13** (81% yield, colorless liquid) was performed according to quaternarization method A and followed by metathesis procedure. ^{1}H NMR (CD_3OD) δ 3.37-3.31 (m, 2H, NCH_2 chain), 3.29-3.24 (m, 2H, NCH_2CH_3), 3.04 (m, 6H, 2×NCH_3), 1.75-1.73 (m, 2H, NCH_2CH_2 chain), 1.38-1.32 (m, 13H, $CH_2CH_2CH_2CH_2CH_2CH_3$, NCH_2CH_3), 0.92-0.89 (m, 3H, $CH_2CH_2CH_3$); ^{13}C NMR (CD_3OD) δ 121.50 and 118.31 (q, $J_{C,F}$= 319 Hz, 2×CF_3), 64.83 (NCH_2 chain), 60.58 (NCH_2CH_3), 50.50 (2×NCH_3), 32.71 (NCH_2CH_2 chain), 30.05 ($NCH_2CH_2CH_2$ chain), 30.01 ($NCH_2CH_2CH_2CH_2$ chain), 27.22 ($CH_2CH_2CH_2CH_3$), 23.51 ($CH_2CH_2CH_3$), 23.34 ($CH_2CH_2CH_3$), 14.26 ($CH_2CH_2CH_3$), 8.24 (NCH_2CH_3); IR (cm^{-1}): 2930.7, 2860.3, 1468.8, 1347.7, 1178.4, 1134.3, 1052.9, 788.8, 739.6 and 614.6. NMR and FTIR are reported in supporting information (Figure S2 and Figure S7).

***N,N*-Diethyl-2-methoxy-*N*-methyl-ethanaminium bis(trifluoromethyl sulfonyl)imide $N_{221,2O1}$ (14).** The preparation of **14** (74% yield, colorless liquid) was performed according to quaternarization method A and followed by metathesis procedure. ^{1}H NMR (CD_3OD) δ 3.78-3.77 (m, 2H, OCH_2), 3.51-3-49 (m, 2H, NCH_2 chain), 3.45-3.42 (m, 4H, 2xNCH_2CH_3), 3.40-3.38 (m, 3H, OCH_3), 3.03 (m, 3H, 2×NCH_3), 1.35-1.30 (m, 6H, NCH_2CH_3); ^{13}C NMR (DMSO-d_6) δ 121.13 and 117.93 (q, $J_{C,F}$= 320 Hz, 2×CF_3), 65.19 (OCH_2), 59.21 (NCH_2 chain), 58.15 (2×NCH_2CH_3), 56.40 (2×NCH_3), 47.17 (OCH_3), 7.47 (NCH_2CH_3); IR (cm^{-1}): 2997.1, 1462.1, 1347.1, 1176.7, 1132.7, 1051.5, 872.1, 788.6, 739.7, 654.2 and 612.6. ^{1}H-NMR, ^{13}C-NMR and FTIR are in accordance with the literature [97].

***N,N*-Diethyl-*N*-methyl-1-butanaminium bis(trifluoromethyl sulfonyl)imide $N_{221,4}$ (15).** The preparation of **15** (81% yield, colorless liquid) was performed according to quaternarization method A and followed by metathesis procedure. ^{1}H NMR (CD_3OD) δ 3.36-3.30 (m, 4H, 2×NCH_2CH_3), 3.25-3.21 (m, 2H, NCH_2 chain), 3.04 (m, 3H, NCH_3), 1.74-1.66 (m, 2H, $NCH_2CH_2CH_2CH_3$), 1.47-1.37 (m, 2H, $NCH_2CH_2CH_2CH_3$), 1.35-1.30 (m, 6H, 3×NCH_2CH_3), 1.04 (m, 3H, $CH_2CH_2CH_3$); ^{13}C NMR (CD_3OD) δ 122.80 and 119.61 (q, $J_{C,F}$= 319 Hz, 2×CF_3), 61.53 (NCH_2 chain), 57.49 (2×NCH_2CH_3), 47.62 (NCH_3), 24.97 (NCH_2CH_2 chain), 20.68 (CH_2CH_3 chain), 13.86 ($CH_2CH_2CH_3$), 7.98 (2×NCH_2CH_3); IR (cm^{-1}): 2969.7, 2881.8, 1470.4, 1347.0, 1175.9, 1133.8, 1051.5, 897.0, 788.6, 739.4, 654.0 and 612.8. ^{1}H-NMR and ^{13}C-NMR are in accordance with the literature [90].

***N,N*-Diethyl-*N*-methyl-1-pentanaminium bis(trifluoromethyl sulfonyl)imide $N_{221,5}$ (16).** The preparation of **16** (78% yield, colorless liquid) was performed according to quaternarization method A and followed by metathesis procedure. ^{1}H

NMR ($CDCl_3$) δ 3.25-3.20 (m, 4H, 2×NCH_2CH$_3$), 3.08-3.03 (m, 2H, NCH_2 chain), 2.84 (m, 3H, NCH_3), 1.62-1.54 (m, 2H, NCH$_2$CH_2 chain), 1.33-1.22 (m, 10H, CH_2CH_2CH$_3$, 2×NCH$_2$CH_3), 0.85-0.81 (m, 3H, CH$_2$CH$_2$CH_3); ^{13}C NMR ($CDCl_3$) δ 121.48 and 118.29 (q, $J_{C,F}$= 319 Hz, 2×CF$_3$), 60.90 (NCH$_2$ chain), 56.62 (2×NCH$_2$CH$_3$), 47.17 (NCH$_3$), 28.11 (NCH$_2$$CH_2$ chain), 21.98 (CH$_2$CH$_2$CH$_3$), 21.68 (CH$_2$$CH_2CH_3$), 13.58 (CH$_2CH_2CH_3$), 7.57 (2×NCH$_2CH_3$); IR (cm^{-1}): 2962.9, 2877.3, 1462.3, 1347.3, 1176.0, 1134.0, 1051.8, 788.6, 739.3, 653.8 and 613.3. ^{1}H-NMR and ^{13}C-NMR are in accordance with the literature [78].

***N,N*-Diethyl-*N*-methyl-1-hexanaminium bis(trifluoromethyl sulfonyl)imide $N_{221,6}$ (17).** The preparation of **17** (84% yield, colorless liquid) was performed according to quaternarization method A and followed by metathesis procedure. ^{1}H NMR (CD_3OD) δ 3.34-3.30 (m, 4H, 2×NCH_2CH$_3$), 3.25-3.21 (m, 2H, NCH_2 chain), 2.97 (m, 3H, NCH_3), 1.72-1.71 (m, 2H, NCH$_2$CH_2 chain), 1.39-1.30 (m, 12H, CH_2CH_2CH_2CH$_3$, 2×NCH$_2$CH_3), 0.95-0.92 (m, 3H, CH$_2$CH$_2$CH_3); ^{13}C NMR (CD_3OD) δ 122.80 and 119.61 (q, $J_{C,F}$= 319 Hz, 2×CF$_3$), 61.74 (NCH$_2$ chain), 57.41 (2×NCH$_2$CH$_3$), 47.60 (NCH$_3$), 32.36 (NCH$_2$$CH_2$ chain), 27.07 (CH$_2$CH$_2$CH$_2$CH$_3$), 23.49 (CH$_2$CH$_2$CH$_3$), 22.99 (CH$_2$$CH_2CH_3$), 14.22 (CH$_2CH_2$$CH_3$), 7.98 (2xNCH$_2$$CH_3$); IR (cm^{-1}): 2934.7, 2864.9, 1462.5, 1347.4, 1176.5, 1134.1, 1052.2, 788.5, 739.1, 653.8 and 613.8. NMR and FTIR are reported in supporting information (Figure S3 and Figure S8).

***N,N*-Diethyl-*N*-methyl-1-octanaminium bis(trifluoromethyl sulfonyl)imide $N_{221,8}$ (18).** The preparation of **18** (65% yield, colorless liquid) was performed according to quaternarization method A and followed by metathesis procedure ^{1}H NMR (CD_3OD) δ 3.32-3.30 (m, 4H, NCH_2CH$_3$), 3.24-3.20 (m, 2H, NCH_2 chain), 2.97 (m, 3H, NCH_3), 1.74-1.69 (m, 2H, NCH$_2$CH_2 chain), 1.40-1.30 (m, 16H, CH_2CH_2CH_2CH_2CH_2CH$_3$, 2×NCH$_2$CH_3), 0.93-0.89 (m, 3H, CH$_2$CH$_2$CH_3); ^{13}C NMR (CD_3OD) δ 122.81 and 119.62 (q, $J_{C,F}$= 319 Hz, 2×CF$_3$), 61.75 (NCH$_2$ chain), 57.47 (NCH$_2$CH$_3$), 47.61 (NCH$_3$), 32.85 (NCH$_2$$CH_2$ chain), 30.20 (NCH$_2$CH$_2$$CH_2$), 30.15 (NCH$_2CH_2CH_2$$CH_2$), 27.39 ($CH_2CH_2CH_2$$CH_3$), 23.64 ($CH_2CH_2CH_3$), 23.04 (CH$_2$$CH_2CH_3$), 14.39 (CH$_2CH_2$$CH_3$), 7.99 (2×NCH$_2$$CH_3$); IR (cm^{-1}): 2930.5, 2860.0, 1462.6, 1347.7, 1177.8, 1134.5, 1052.8, 788.5, 739.3, 653.7 and 614.4. NMR and FTIR are reported in supporting information (Figure S4 and Figure S9).

2-Ethoxy-*N,N*-diethyl-*N*-methyl-ethanaminium bis(trifluoromethyl sulfonyl)imide $N_{221,2O2}$ (19). The preparation of **19** (71% yield, yellowish liquid) was performed according to quaternarization method A and followed by metathesis procedure. ^{1}H NMR (CD_3OD) δ 3.82-3.81 (m, 2H, OCH_2CH$_3$), 3.57-3-54 (m, 2H, OCH_2CH$_2$), 3.52-3.41 (m, 6H, 3×NCH_2), 3.04 (m, 3H, NCH_3), 1.36-1.31 (m, 6H, 2×NCH$_2$CH_3), 1.22-1.20 (m, 3H, OCH$_2$CH_3); ^{13}C NMR (DMSO-d$_6$) δ 121.09 and 117.89 (q, $J_{C,F}$= 320 Hz, 2×CF$_3$), 65.70 (OCH$_2$CH$_3$), 63.07 (OCH$_2$CH$_2$), 59.22 (NCH_2 chain), 56.37 (2×NCH_2CH$_3$), 47.21 (NCH$_3$), 14.80 (OCH$_2$$CH_3$), 7.53 (2×NCH$_2$$CH_3$); IR (cm^{-1}): 2984.2, 2881.5, 1462.5, 1347.5, 1176.9, 1132.2, 1051.3, 866.9, 788.2, 739.5, 654.0, 612.6 and 569.1. NMR and FTIR are reported in supporting information (Figure S5 and Figure S10).

***N,N*-Diethyl-2-(2-methoxyethoxy)-*N*-methyl-ethanaminium bis(trifluoromethyl sulfonyl)imide $N_{221,2O2O1}$ (20).** The preparation of **20** (10% yield, white solid) was performed according to quaternarization method B and followed by metathesis procedure. ^{1}H NMR (CD_3OD) δ 3.90-3.88 (m, 2H, NCH$_2$CH$_2$OCH_2), 3.64-3.66 (m, 2H, CH_2OCH$_3$), 3.57-3.54 (m, 2H, NCH$_2$CH_2O), 3.52-3.50 (m, 2H, NCH_2CH$_2$O), 3.47-3.42 (m, 4H, 2×NCH_2CH$_3$), 3.37 (m, 3H, OCH_3), 3.04 (m, 3H, NCH_3),1.36-1.31 (m, 6H, 2×NCH$_2$CH_3); ^{13}C NMR (CD_3OD) δ 121.50 and 118.32 (q, $J_{C,F}$= 318 Hz, 2×CF$_3$), 71.45 (NCH$_2$CH$_2$OCH$_2$), 69.98 (CH$_2$OCH$_3$), 64.14 (NCH$_2$$CH_2$O), 59.92 (N$CH_2CH_2$O), 57.80 (2×N$CH_2CH_3$), 57.32 (O$CH_3$),

53.26 (N*C*H_3), 6.83 (NCH$_2$*C*H_3); IR (cm^{-1}): 2921.0, 1463.0, 1347.3, 1177.8, 1132.9, 1051.6, 871.6, 788.8, 739.6, 654.3 and 612.0. ^{1}H-NMR is in accordance with the literature [98].

***N*-Diethyl-*N*-(methoxymethyl)-*N*-methyl-ethanaminium bis(trifluoromethyl sulfonyl)imide $N_{221,1O1}$ (21).** The preparation of **21** (65% yield, yellowish liquid) was performed according to quaternarization method C and followed by metathesis procedure. ^{1}H NMR (DMSO-d$_6$) δ 4.57 (m, 2H, OC*H*$_2$N), 3.57 (m, 2H, OC*H*$_3$), 3.28-3.25 (m, 4H, 2xNC*H*$_2$CH$_3$), 2.87 (m, 3H, NC*H*$_3$), 1.22-1.19 (m, 6H, 2×NCH$_2$C*H*$_3$); ^{13}C NMR (DMSO-d$_6$) δ 121.11 and 117.91 (q, $J_{C,F}$= 320 Hz, 2×*C*F$_3$), 88.11 (O*C*H$_2$N), 60.04 (O*C*H$_3$), 53.09 (2×N*C*H$_2$CH$_3$), 43.62 (N*C*H$_3$), 7.20 (2×NCH$_2$*C*H$_3$); IR (cm^{-1}): 2995.6, 1463.6, 1398.7, 1347.3, 1175.9, 1132.5, 1051.0, 788.7, 739.8, 654.3 and 612.5. ^{1}H-NMR, ^{13}C-NMR and FTIR are in accordance with the literature [99].

2-Methoxy-*N,N,N*-trimethyl-ethanaminium bis(trifluoromethyl sulfonyl)imide $N_{111,2O1}$ (22). The preparation of **22** (71% yield, white solid) was performed according to quaternarization method C and followed by metathesis procedure. ^{1}H NMR (CD$_3$OD) δ 3.84-3.80 (m, 2H, OC*H*$_2$), 3.58-3.56 (m, 2H, NC*H*$_2$CH$_2$O), 3.39 (m, 3H, OC*H*$_3$), 3.18 (m, 9H, 3×NC*H*$_3$); ^{13}C NMR (CD$_3$OD) δ 122.69 and 119.50 (q, $J_{C,F}$= 319 Hz, 2×*C*F$_3$), 67.08 (O*C*H$_2$), 66.77 (N*C*H$_2$CH$_2$O), 58.98 (O*C*H$_3$), 54-58-54.50 (3×N*C*H$_3$); IR (cm^{-1}): 2956.0, 2897.4, 1478.1, 1349.5, 1319.0, 1180.6, 1136.0, 1052.2, 957.3, 941.6, 874.1, 790.5, 740.5, 610.9 and 568.4. ^{1}H-NMR is in accordance with the literature [77].

***N,N,N*-Trimethyl-1-octanaminium bis(trifluoromethyl sulfonyl)imide $N_{111,8}$ (23).** The preparation of **23** (84% yield, yellowish liquid) was performed according to metathesis procedure starting from the commercial bromide product. ^{1}H NMR (CD$_3$OD) δ 4.79 (m, 2H, NC*H*$_2$CH$_2$), 3.11-3-10 (m, 9H, 3×NC*H*$_3$), 1.78-1.76 (m, 2H, NCH$_2$C*H*$_2$), 1.38-1.32 (m, 10H, C*H*$_2$C*H*$_2$C*H*$_2$C*H*$_2$C*H*$_2$CH$_3$), 0.92-0.89 (m, 3H, CH$_2$C*H*$_3$); ^{13}C NMR (CD$_3$OD) δ 122.79 and 119.60 (q, $J_{C,F}$= 319 Hz, 2×*C*F$_3$), 67.92 (N*C*H$_2$CH$_2$), 53.51 (3×N*C*H$_3$), 32.79 (NCH$_2$*C*H$_2$), 30.12 (NCH$_2$CH$_2$*C*H$_2$), 30.06 (NCH$_2$CH$_2$CH$_2$*C*H$_2$), 27.24 (*C*H$_2$CH$_2$CH$_2$CH$_3$), 23.87 (*C*H$_2$CH$_2$CH$_3$), 23.59 (*C*H$_2$CH$_3$), 14.36 (CH$_2$*C*H$_3$); IR (cm^{-1}): 2930.7, 2860.5, 1481.7, 1347.2, 1178.7, 1134.2, 1052.9, 969.2, 908.5, 789.2, 739.8 and 614.2. ^{1}H-NMR is in accordance with the literature [100].

2.2.2 NMR spectroscopy

The NMR spectra were recorded using a Bruker Avance II NMR spectrometer operating at 400 (^{1}H) and 100 MHz (^{13}C) at 24 °C. NMR samples have been prepared dissolving about 20 mg of ILs in a suitable deuterated solvent (around 0.4 mL). ^{1}H and ^{13}C NMR chemical shifts (ppm) are referenced to the residual deuterated solvent signals of CD$_3$OD (^{1}H 3.31 ppm, ^{13}C 49.0 ppm), DMSO-d$_6$ (^{1}H 2.49 ppm, ^{13}C 39.50 ppm) and CDCl$_3$ (^{1}H 7.26 ppm, ^{13}C 77.00 ppm). The following abbreviation was used m=multiplet, and the coupling constants (J) are expressed in Hertz (Hz).

2.2.3 Fourier transform infrared spectroscopy (FTIR)

The ATR-FTIR spectra were recorded with an Agilent Technologies IR Cary 660 FTIR spectrophotometer using a diamond crystal's macro-ATR accessory. The spectra were measured in a range from 4000 to 500 cm^{-1} with 32 scans and a resolution of 4 cm^{-1}.

2.2.4 Differential scanning calorimetry (DSC)

The thermal behavior of the prepared compounds was analyzed by a differential scanning calorimeter (TA DSC, Q250, USA, temperature accuracy ±0.05 °C and temperature precision ±0.008 °C). Dry high purity N_2 gas with a flow rate of 50 cm^3 min^{-1} was purged through the sample. The temperature calibration was performed considering the heating rate dependence of the onset temperature of the melting peak of indium. About 1-3 mg of each sample was loaded in pinhole hermetic aluminum crucibles. The phase behavior was explored under a nitrogen atmosphere in the temperature range between -90 °C and 150 °C. DSC experiments were carried out in duplicate. T_g was obtained by taking the midpoint of the heat capacity change on heating from a glass to a liquid. T_{cc} was determined as the peak temperature of the exothermic peak on heating from a subcooled liquid to a crystalline solid. T_m was taken as the peak temperature of the endothermic peak on the heating run. The peak temperatures were chosen instead of the onset temperatures due to the complexity of the thermograms.

2.2.5 Electrochemical analysis

The electrochemical stability window of the prepared compounds was evaluated at -33 °C by means of linear sweep voltammetry, using two-electrode test cells and an Agilent B2912 source-measure unit. The working temperature of -33 °C was selected since it is sufficiently below 0 °C so as to be suitable for ionic gating applications where low temperatures are used to quench undesired electrochemical reactions, while at the same time it allows for all the ILs considered in this work to exhibit an ionic conductivity large enough to result in a detectable ionic current upon voltage polarization. The test cells consist of two asymmetric gold electrodes obtained by thermal evaporation through a shadow mask on thin glass slides. In all cells, the working electrode area was ~1% of the counter electrode area so that the capacitance of the latter did not contribute to the current dynamics. The compounds were drop casted on the test cells, then loaded on the cold finger of a Cryomech pulse-tube cryocooler and left to degas in a high vacuum (residual pressure < 10^{-5} mbar) at least 2 days before cooling the system to the working temperature to remove absorbed moisture. Fresh cells were utilized for all voltammetry tests to determine the cathodic and anodic stability limits separately. The measurements were performed by grounding the working electrode and sweeping the counter electrode potential from 0 to positive (cathodic limit, up to +10 V) or negative (anodic limit, up to -10 V) voltage values. The applied sweep rate was 5 mV s^{-1} in all cases. The potentials corresponding to the onset of reductive/oxidative decomposition of the electrolyte were estimated by linearly fitting the current-voltage curves in the voltage ranges where the current exhibited a good linear scaling with increasing voltage (using a Levenberg-Marquardt algorithm as implemented in the OriginLab software) and then performing a linear regression to zero current.

3. Results and discussion

This work aims at identifying possible guidelines for developing ILs suitable for applications as gating agents at low temperatures (-33 °C) in electrochemical transistors where the kinetics of chemical reactions are reduced or suppressed. Therefore, ILs were selected to develop a systematic approach to understand the correlation between molecular structure and electrochemical stability. The ILs were characterized by DSC to select the compounds suitable to work at temperatures below -50 °C to allow the measurement of the electrochemical windows at -33 °C. Afterwards, the electrochemical stability was measured. Some of these ILs are not reported in the literature and were prepared to fill the

knowledge gap and have a clearer picture of the correlation between EW and molecular structure. As far as we know, no analysis of the electrochemical stability for these systems at temperatures below 0 °C is reported in the literature.

3.1 Synthesis of compounds

Ammonium cations with three "short chains" and a "long chain" were studied in this work. The short chains were selected using six common tertiary amines (methyl-piperidine, methyl-pyrrolidine, triethylamine, dimethylethylamine, diethylmethylamine and trimethylamine), and the long chains were added using alkyl- and ether- chains using the corresponding bromide chains. The Tf_2N was selected as the anion due to its high-performance properties already described in the Introduction. The synthesis of the ILs is shown in Scheme 1.

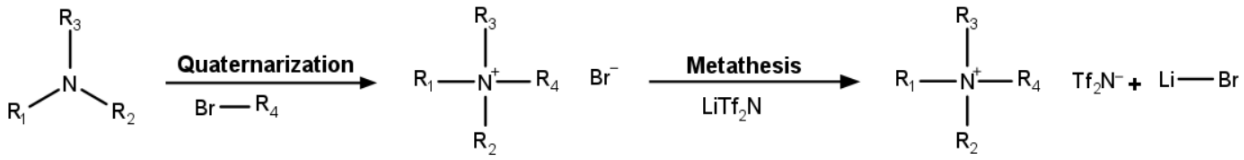

Scheme 1. Synthetic approach for the preparation of the ILs

The molecular structure of the cations and the anion studied in this work are reported in Figure 1.

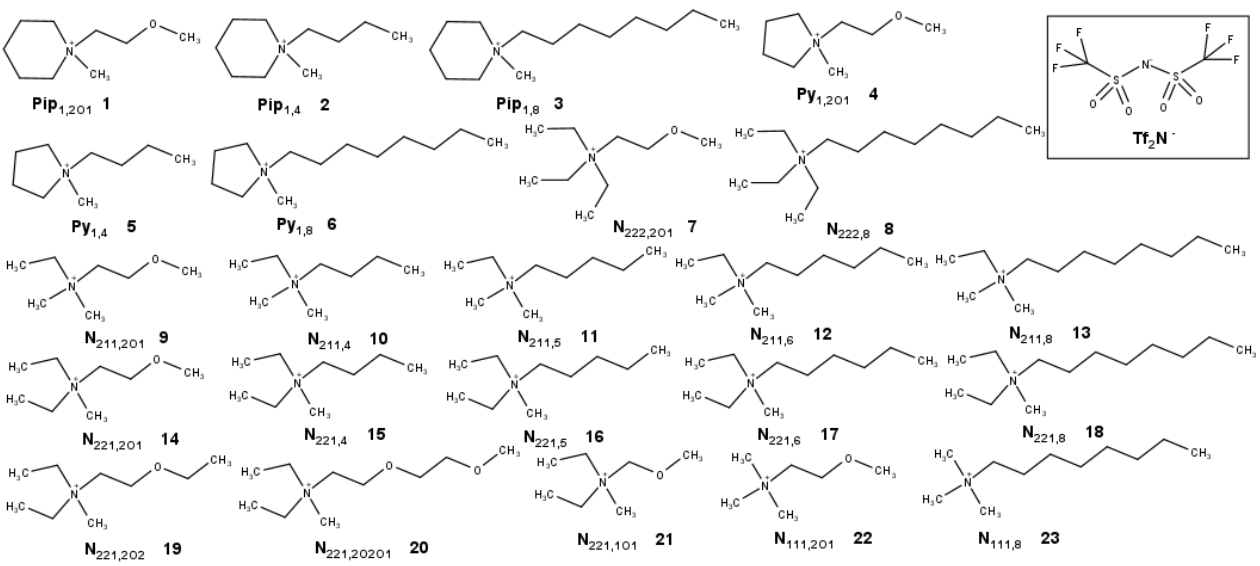

Figure 1. Cations and Anion studied in this work.

The first step consists in ILs quaternarization (also called Menshutkin reaction), a bimolecular nucleophilic substitution of type 2 (S_N2) [101]. In this work, tertiary amine reacted with bromide compounds to obtain a salt composed of quaternary ammonium and bromide ions. Acetonitrile and tetrahydrofuran were used as solvents in almost all the reactions. Only in the case of the Quaternarization Method D water was used as a solvent because the starting trimethylamine dissolved in water allowed a higher concentration of amine than other solvents. The second stage was the anion metathesis reaction, which consists of ion exchange. In this work, the quaternary ammonium cations exchanged the bromide anion with Tf_2N

[102]. The ILs were characterized using NMR and FTIR. The spectra of the ILs not described in the literature are reported in the Supporting Information.

3.2 Thermal analysis

The thermal behavior was evaluated using DSC. The analysis was performed under a nitrogen flow, and the temperature range was from -90 °C to 150 °C with a scan speed of 10 °C min^{-1}. At first, the sample was cooled down from 40 °C to -90 °C and maintained at this temperature for 3 min. Then, it was heated to 150 °C to ensure the complete sample melting (1st heating run). Afterwards, the sample was subjected to the 2nd cycle of cooling-heating to compare the thermal behavior of the studied compounds. The obtained thermograms are reported in Figures S11-S33 in the supporting information, while the values of the transitions are reported in Table 1.

Table 1. DSC data from thermograms of compounds **1-23**. In blue are reported data from the first cycle, and in green, data from the second cycle. T_g (glass transition temperature), T_{cc} (cold crystallization temperature), T_m (melting temperature) and T_c (crystallization) during the cooling cycle.

ILs	T_g (°C)		T_{cc} (°C)		T_m (°C)		2nd T_m (°C)		T_c (°C)	Thermal behavior
$Pip_{1,2O1}$ (1)	-77.21	-76.61								I
$Pip_{1,4}$ (2)	-72.13	-71.51								I
$Pip_{1,8}$ (3)	-68.75	-68.64								I
$Py_{1,2O1}$ (4)	-83.20	-82.91								I
$Py_{1,4}$ (5)			-53.43	-52.3	-26.62	-26.22	-18.62	-17.91		III
$Py_{1,8}$ (6)	-79.52	-79.4		-24.33		-14.21				III
$N_{222,2O1}$ (7)	-79.05	-78.33	-33.54	-32.73	24.43	24.95				III
$N_{222,8}$ (8)	-72.63	-72.67								I
$N_{211,2O1}$ (9)										n.c.*
$N_{211,4}$ (10)										n.c.*
$N_{211,5}$ (11)	-82.61	-82.43	-27.57	-25.96	-7.97	-7.79				III
$N_{211,6}$ (12)	-82.53	-82.05								I
$N_{211,8}$ (13)	-81.17	-80.78								I
$N_{221,2O1}$ (14)										n.c.*
$N_{221,4}$ (15)				-36.39		11.19				III
$N_{221,5}$ (16)	-84.36	-83.8								I
$N_{221,6}$ (17)	-82.75	-82.66								I
$N_{221,8}$ (18)	-80.65	-80.48								I
$N_{221,2O2}$ (19)										n.c.*
$N_{221,2O2O1}$ (20)		-63.13		-13.35	36.01	34.91	70.59	71.31	-16.64	II
$N_{221,1O1}$ (21)			-51.17		-31.42					n.c.
$N_{111,2O1}$ (22)					38.93	38.36			-24.58	II
$N_{111,8}$ (23)	-73.6	-72.29	-33.06		5.38					I

*n.c.= not classified because the transitions are not detected in the studied temperature range.

Based on the results shown in Table 1, all the salts studied in this work can be classified as ILs because they melt at temperatures below 100 °C [67]. Three kinds of thermal behaviors have been generally observed for ILs [103]:

- Type I, only the formation of amorphous glassy solids is displayed.

- Type II, the presence of a crystallization event during the cooling run and a corresponding melting transition during the heating run.
- Type III, only a crystallization is observed in the heating run (cold crystallization), which is inhibited during the cooling run.

Based on the second cycle of the DSC, the ILs of this study case can be classified as reported in Table 1.

3.2.1 Thermal behavior of cyclic tertiary amines

The cyclic tertiary amines (**Pip$_{1,2O1}$**, **Pip$_{1,4}$**, **Pip$_{1,8}$**, **Py$_{1,2O1}$**, **Py$_{1,4}$** and **Py$_{1,8}$**) show a similar transition temperature with respect to the literature [89,104,105]. The lowest transition temperature is recorded for **Pip$_{1,2O1}$** (-76.91 °C) and **Py$_{1,2O1}$** (-82.91 °C) with ether chain. Also, **Py$_{1,4}$** and **Py$_{1,8}$** (-17.91 °C and -14.21 °C) show higher transition temperatures than **Pip$_{1,4}$** and **Pip$_{1,8}$** (-71.51 °C and -68.64 °C). Therefore, it is possible to consider that the pyrrolidinium-based ILs allow the formation of more organized and crystalline structures in the case study.

3.2.2 Thermal behavior of linear tertiary amines

The linear tertiary amines (**N$_{222,2O1}$**, **N$_{222,8}$**, **N$_{211,5}$**, **N$_{221,4}$**, **N$_{111,2O1}$** and **N$_{111,8}$**) show a thermal behavior similar to the literature [77,78,83,106]. **N$_{211,2O1}$** and **N$_{221,2O1}$** did not display a transition temperature, but a T_g= -96 °C and -95 °C are reported in the literature [77], respectively. Similarly, a transition temperature was not reported for **N$_{211,4}$**, probably because lower than -90 °C; this result agrees with Le *et al.* [107]. The thermal behavior of ILs **N$_{211,6}$**, **N$_{211,8}$**, **N$_{221,5}$**, **N$_{221,6}$**, **N$_{221,8}$**, **N$_{221,2O2}$**, **N$_{221,2O2O1}$** and **N$_{221,1O1}$** is not reported in the literature.

Based on the second cycle of the DSC, it is possible to observe that an increase in the overall symmetry of cation structures allows the formation of organized structures. Consequently, the T_g increases when the length of the long alkyl chain is not so different from the one of the short chains. However, a clear correlation between the length of the alkyl long chain and the transition temperature is not observed. Secondly, oxygen in the chain decreases the transition temperature of the ILs when one of the short alkyl chains has a different length from the other two, and the ether chain has 3-5 atoms. Furthermore, three ether chains were studied for this type of ILs (**N$_{221,2O1}$**, **N$_{221,2O2O1}$** and **N$_{221,1O1}$**). In this case, the presence of a long ether chain determines the formation of a solid. In fact, the **N$_{221,2O2O1}$** shows a high melting point at 71.31 °C.

In conclusion, **N$_{221,1O1}$** and **N$_{111,8}$** showed a variation in the thermal behavior between the first and the second cycles, differently from the other ILs. A melting point at -31.42 °C and 5.38 °C, respectively, was observed only during the first cycle. This transition was not observed during the second cycle when ILs were already melted. It means that the first cycle allows eliminating the thermal memory of the sample due to the synthesis process.

3.2.3 Selection of ILs for electrochemical analysis

At the end of the thermal analysis, the most suitable ILs to work as gating agents at low temperatures (-33 °C) were selected. The ILs must keep the liquid state during the electrochemical analysis because a solidification causes a drastic conductivity decrease, impeding a correct analysis of the sample. The range where the 23 ILs are in the liquid state is

illustrated in Figure 2. Upper limit: 150 °C (maximum temperature to classify a transistor as traditional [108]); in the present study, all ILs studied showed stability until this temperature. Lower limit: it was defined as the T_{peak} (T_m or T_g) during the second cycle of DSC. In the case of the ILs that did not show a transition temperature, the minimum limit was arbitrarily defined as -90 °C (the limit of DSC analysis). The electrochemical stability of ILs marked in green in Figure 2 can be measured at a low temperature (-33 °C). The compounds marked in blue can be used at low temperatures when they are first melted to eliminate the thermal memory. The ILs marked in red cannot be used as ionic gating agents at low temperatures because they show a transition temperature (T_{cc}, T_m or T_g) above -50 °C. The piperidine-like compounds **Pip$_{1,2O1}$ (1)**, **Pip$_{1,4}$ (2)** and **Pip$_{1,8}$ (3)** can operate at -33 °C. Instead, **Py$_{1,2O1}$ (4)** is the only pyrrolidinium-based ILs that can work at -33 °C. About the linear tertiary amines having short chains with the same length, both ILs having long alkyl chains, **N$_{222,8}$ (8)** and **N$_{111,8}$ (23)**, show transition temperatures that allow the operability at -33 °C. For linear tertiary amines having a short chain with different lengths from the other two, the ILs **N$_{211,5}$ (11)**, **N$_{221,4}$ (15)** and **N$_{221,2O2O1}$ (20)** cannot operate at -33 °C.

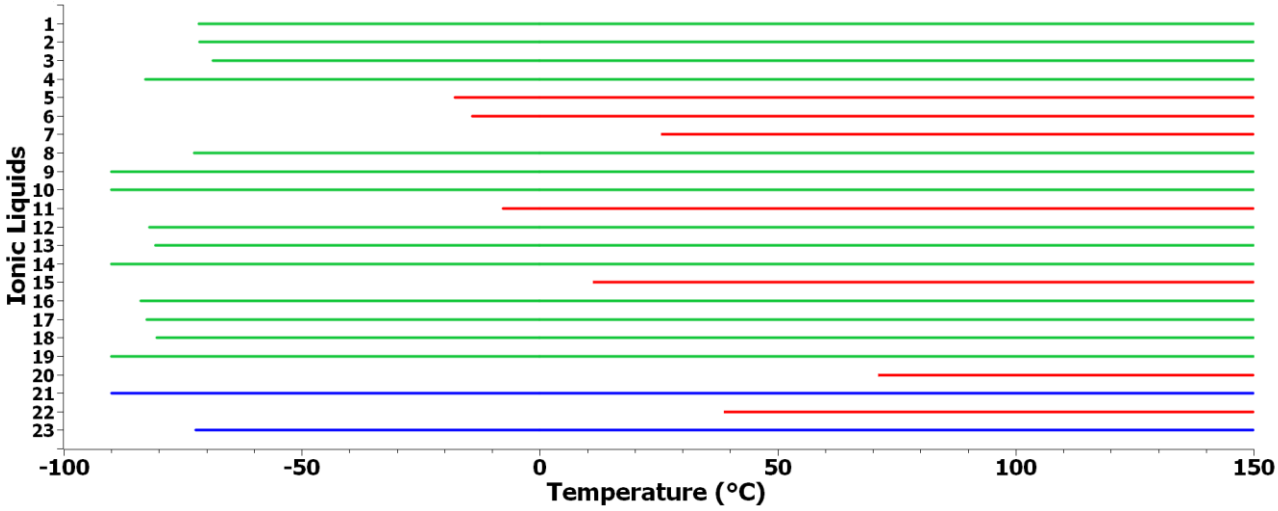

Figure 2. Classification of the 23 ILs studied in this work depending on their liquid range. Green line: ILs which are liquids below -50 °C. Blue line: ILs which are liquids below -50 °C, albeit require a preheating step. Red line: ILs which are liquids at temperatures above -50 °C. 150 °C is the temperature limit for the classification of traditional temperature transistors.

3.3 Electrochemical analysis

Electrochemical stability is the potential range where the electrolytes do not go under reductive or oxidative decompositions [76]. The typical electrochemical measurements are realized via either linear-sweep [77,109] or cyclic [72,76] voltammetry using three-electrode cells (a working and counter electrodes having equal areas and a reference electrode) by grounding the counter electrode and sweeping the working electrode potential from the open-circuit voltage towards more negative (cathodic) or more positive (anodic) potentials. In electrochemical transistors, the reference electrode is often missing, and the working electrode (coinciding with the active channel of the transistor) is kept grounded. At the same time, the potential of the counter electrode is controlled via the gate voltage by sweeping it from zero to either positive (cathodic) or negative (anodic) values [110]. Additionally, the counter electrode area is typically much larger than the area of the working electrode, so the counter electrode capacitance is so large as to be negligible in determining both the switching dynamics and the potential distribution inside the gate loop [111]. Since the goal of our

work is determining values of electrochemical stability relevant for electrochemical transistors, this latter configuration was mimicked in the linear-sweep voltammetry measurements carried out in this study by making use of two-electrode test cells with a counter electrode-working electrode area ratio of 100:1, keeping the working electrode grounded and sweeping the counter electrode potentials from zero to either positive or negative values. Gold was selected as a material for both electrodes as it is ubiquitously employed in electrochemical transistors both for the counter electrode and for the electrical leads to the active channel [112]. The obtained voltammograms are illustrated in Figures S34-S49 in the supporting information, and the data about the electrochemical stability are reported in Table 2 and Figure 3.

Table 2. Electrochemical stability of compounds **1-23**.

IL	Cathodic stability limit (V>0)	Std Dev (+)	Anodic stability limit (V<0)	Std Dev (-)
$Pip_{1,2O1}$ (1)	5.1	0.1	-4.6	0.1
$Pip_{1,4}$ (2)	4.1	0.1	-4.9	0.1
$Pip_{1,8}$ (3)	3.8	0.1	-2.9	0.2
$Py_{1,2O1}$ (4)	5.5	0.1	-4.8	0.2
$N_{222,8}$ (8)	4.3	0.2	-3.3	0.2
$N_{211,2O1}$ (9)	5.7	0.1	-4.6	0.1
$N_{211,4}$ (10)	5.3	0.1	-5.1	0.1
$N_{211,6}$ (12)	5.1	0.1	-5.2	0.1
$N_{211,8}$ (13)	5.0	0.1	-4.0	0.2
$N_{221,2O1}$ (14)	5.5	0.1	-4.9	0.3
$N_{221,5}$ (16)	5.3	0.1	-5.0	0.3
$N_{221,6}$ (17)	5.0	0.1	-5.0	0.1
$N_{221,8}$ (18)	4.1	0.2	-4.4	0.2
$N_{221,2O2}$ (19)	5.4	0.1	-3.7	0.1
$N_{221,1O1}$ (21)	5.3	0.1	-3.6	0.1
$N_{111,8}$ (23)	3.9	0.1	-3.4	0.2

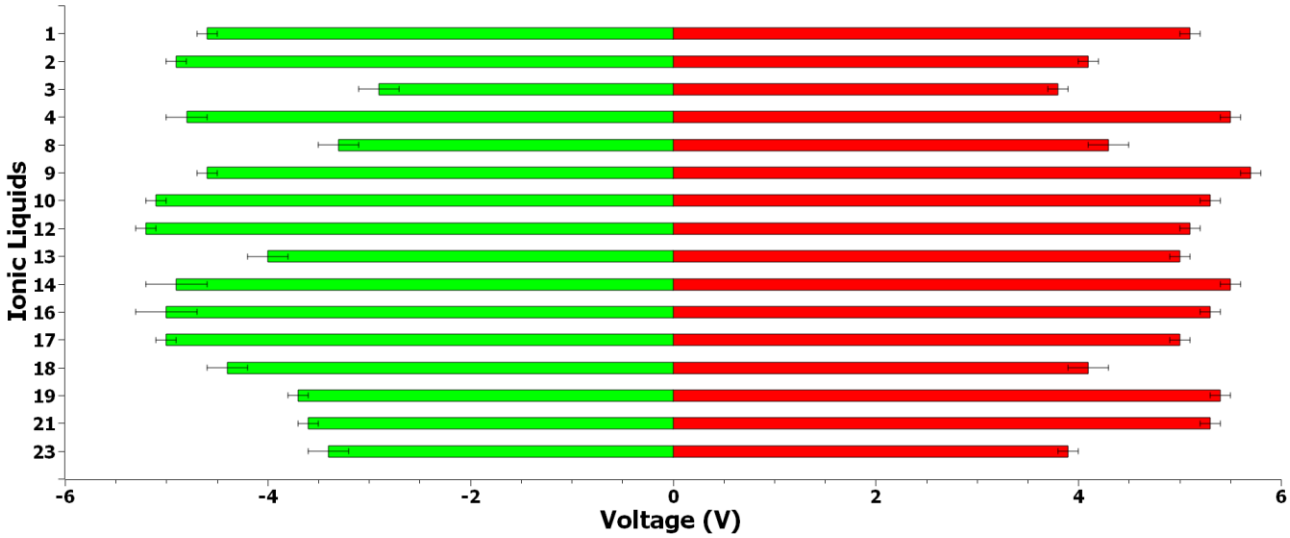

Figure 3. Values of Cathodic and Anodic limits of ILs. Green: Anodic stability limit, Red: Cathodic stability limit

3.3.1 Effect of the long chain

Different authors reported that the anodic stability depends on the length of the longest alkyl chain of the ILs based on aliphatic quaternary ammonium salts [77,83]. The shorter it is, the higher is the oxidation potential. Phung *et al.* [83] correlated this behavior with the HOMO value determined using Density Functional Theory (DFT) calculations that decrease with the alkyl chains' reduction. The lower the HOMO energy is, the higher the quaternary ammonium stability is. In the case of piperidinium cations, it was observed that the cathodic limit becomes wider, increasing the main alkyl chain length, while the anodic limit is almost stable. For the authors, these results indicate that the electrochemical stability of these ILs is mainly governed by the reduction of the piperidinium-based cation structure. The main-alkyl-chain length probably plays a shielding effect of the positively-charged nitrogen. Also, the length of the alkyl chain helps to stabilize the aliphatic free radicals generated during the electrochemical reduction [84]. As reported in Figure 3, the increase of alkyl long chain length decreases the stability windows for both cathodic and anodic voltages. This behavior is more evident in the cathodic voltages than in the anodic side. Also, this decrease in electrochemical stability is marked when the alky chains having a number of carbon atoms equal to or below six, such as **$N_{211,4}$ (10)**, **$N_{211,6}$ (12)**, **$N_{221,5}$ (16)** and **$N_{221,6}$ (17)**, are compared to the alkyl chains with eight carbon atoms, **$N_{211,8}$ (13)** and **$N_{221,8}$ (18)**. Moreover, there is no evident difference between the dimethyl-ethylamine and diethyl-methylamine derivatives ILs except for the cathodic limit of ILs having an alkyl chain with eight carbon atoms **$N_{211,8}$ (13)** and **$N_{221,8}$ (18)**. The aliphatic quaternary ammonium salts show the same behavior with respect to the literature. The piperidinium-based ILs, **$Pip_{1,4}$ (2)** and **$Pip_{1,8}$ (3)** have low cathodic limits, and the latter shows the lowest electrochemical stability. In this case, the piperidinium-based cations show different behavior with respect to the literature. However, only two piperidinium derivatives were studied, and the difference in the determination of electrochemical stability does not allow us to reach conclusions. About the variation of ether chains, Figure 4 shows that **$N_{221,2O1}$ (14), $N_{221,2O2}$ (19)** and **$N_{221,1O1}$ (21**) have similar cathodic limits. Also, the **$N_{221,2O1}$ (14)** shows a higher anodic limit than the other two ILs. This result contrasts with Nokami *et al*. [87], who observed that the anodic potential increased with an ether chain having an oxygen atom close to the nitrogen atom. This difference can be correlated to the difference in the measurement of electrochemical stability and the quaternarization method of **$N_{221,1O1}$ (21)**, which can cause the presence of impurities that can influence the electrochemical windows [69].

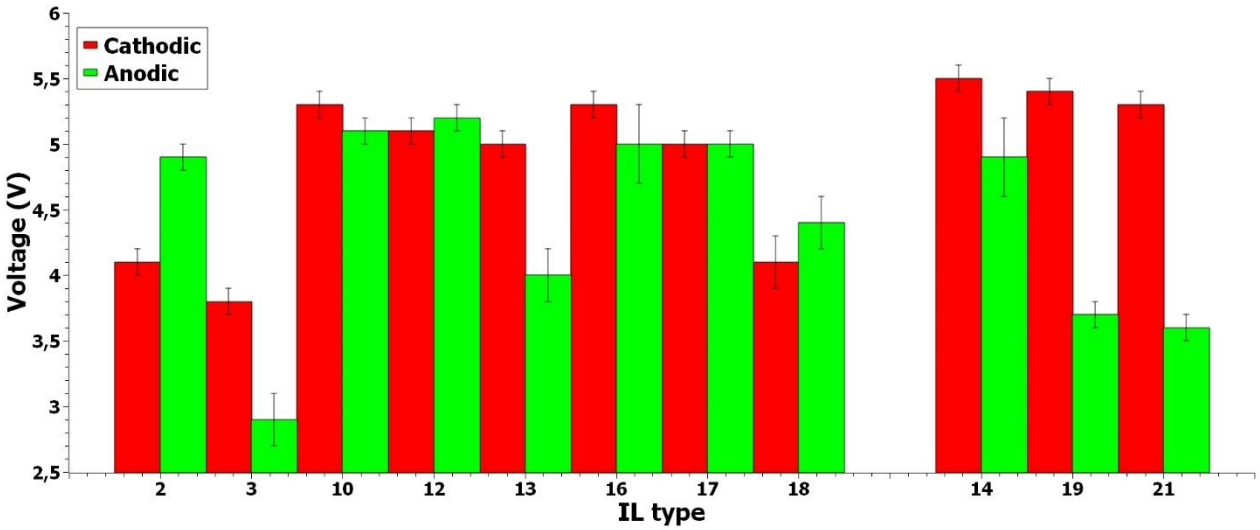

Figure 4. Absolute values of cathodic (red) and anodic (green) limits of ILs having the same short chains and increasing the long chain.

3.3.2 Comparison of long ether chains versus long alkyl chains having the same length and same short chains

The ether functionalities reported in the literature exhibit lower electrochemical stability than alkyl groups having the same length [76,77,85,86]. Neale *et al.* [76] justify this behavior because the ionicity of the ILs decreases by adding ethereal groups to the alkyl chain. The presence of an electron donor group decreases the delocalization of the positive charge present in the cation, reducing its stability. Appetecchi *et al.* [85] explain this behavior by the electrostatic interactions between the lone-pair electrons of oxygen and positively-charged nitrogen. These interactions decrease the electron density of the oxygen, promoting the reduction of the alkoxy ethyl chain. Zhou *et al.* [77] found that it was necessary to increase the size of the cations with longer side alkyl chains to "bury" the positive charge on the nitrogen when an ether chain is added. However, as reported in Figure 5, the cathodic windows of ether chains ILs look higher than the ones of alkyl chain compounds. On the contrary, ILs having alkyl chains show wider anodic limits than ILs with ether chains. This divergence from the literature could be correlated to the different experimental conditions where the electrochemical stability was measured. At lower temperatures, ethers become "more resistant" to reduction reactions. **$Pip_{1,4}$ (2)** has lower cathodic and anodic limits than aliphatic ammonium cations, **$N_{211,4}$ (10)** and **$N_{221,5}$ (16)**, although the latter has longer long alkyl chain. Moreover, **$N_{211,2O1}$ (9)** shows the highest cathodic limit. **$N_{221,2O2}$ (19)** shows a higher cathodic limit than **$Pip_{1,2O1}$ (1)** despite the longer ether chain. On the contrary, **$Pip_{1,2O1}$ (1)** has an anodic limit comparable with **$N_{211,2O1}$ (9).**

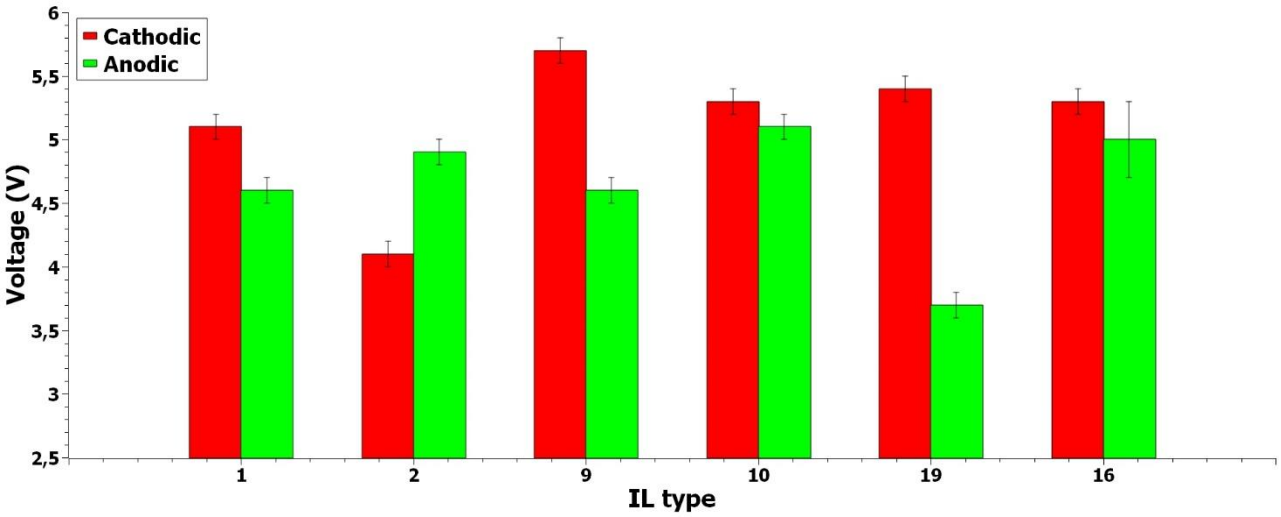

Figure 5. Absolute values of cathodic (red) and anodic (green) limits of ILs to compare alkyl and ether long chains having the same length.

3.3.3 Effect of the short chains

Phung *et al.* [83] observed that with the same longest-chain length, the oxidation stability depends on the other alkyl-chain length, showing wider stability when the side alkyl chains are as short as possible. However, this aspect is not discussed in detail because only two tertiary amines were studied. As reported in Figure 6, **$N_{211,8}$ (13)** shows the highest cathodic window and the second-highest anodic window. On the other hand, the **$N_{221,8}$ (18)** presents the highest anodic window and the second-highest cathodic window together with **$N_{222,8}$ (8)**. Instead, **$Pip_{1,8}$ (3)** shows the lowest electrochemical windows. These results indicate that both anodic and cathodic voltage limits are influenced by the type of short chains of the ammonium cations. At the same time, it is possible to observe that the presence of short chains

having different lengths allowed to obtain wider electrochemical stability. About the ether functionalities, the **$N_{211,2O1}$ Tf_2N** shows the highest cathodic window, followed by the **$N_{221,2O1}$ Tf_2N** and **$Py_{1,2O1}$ Tf_2N**. The similarity between compounds **$N_{221,2O1}$ Tf_2N** and **$Py_{1,2O1}$ Tf_2N** can be justified by their similar structure; the methyl-pyrrolidine is a "closed ring" of the diethyl-methylamine. The **$Pip_{1,2O1}$ Tf_2N** shows the lowest electrochemical window. About the anodic limit, the variation of the windows is inside the standard error of the measurement, as reported in Table 2. As previously observed, short chains with different lengths allowed for obtaining wider electrochemical stability. Moreover, the presence of the ether chain allows a pyrrolidinium-based cation to work at low temperatures, which was not possible using long alkyl chains.

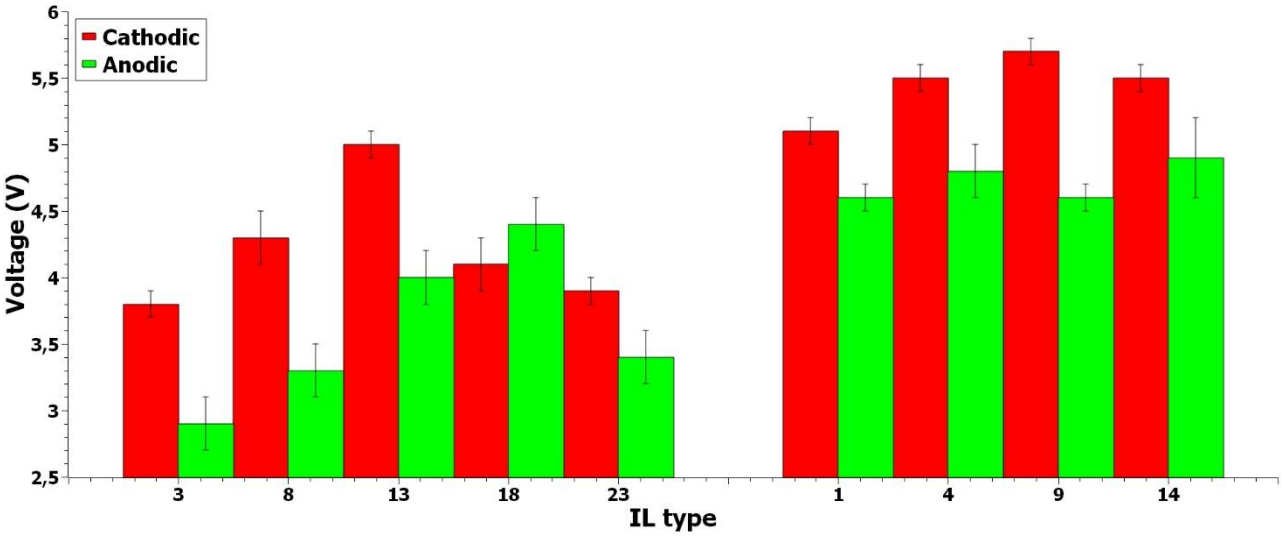

Figure 6. Absolute values of cathodic (red) and anodic (green) limits of ILs having the same long chain and changing the short chains.

4. Conclusion

In summary, our work establishes five main guidelines for the selection of ILs based on ammonium cations and Tf_2N anion, suitable as gating agents for transistors-like systems at low temperatures:

1. The cations and the anions cannot be considered separately. As observed by Zhao *et al*., the association of anions or cations plays an essential role in their electrochemical stabilities [73].
2. The ammonium cations having short chains with different lengths show larger electrochemical stability for the cathodic and anodic limits than ammonium cations having short chains with the same length. As best of our knowledge, this is the first article that studies and describes the effect of the short chains.
3. The increase of the "long chain" length decreases the electrochemical stability for both cathodic and anodic limits. This result is comparable with the literature for the linear tertiary amine [77,83]. At the same time, the results for the piperidinium-based ILs are in contrast with the literature [84].
4. The presence of an oxygen atom in the "long chain" increases the cathodic limit but decreases the anodic limit. The behavior in the cathodic limit is in contrast with the literature, where it is described as a decrease in electrochemical stability [76,77,85,86].
5. The ether length composed of three carbon atoms and one oxygen showed larger electrochemical stability than other ethers having two or four carbon atoms. The larger electrochemical stability of IL **$N_{221,2O1}$ (14)** with respect

to **$N_{221,1O1}$ (21**) is in contrast with the results of Nokami *et al.,* who determined that the oxygen atom located far from the nitrogen atom decreased the anodic limit [87].

In conclusion, the IL having the widest cathodic and anodic limits observed during this study were **$N_{211,2O1}$ (9)** and **$N_{211,6}$ (12)**, respectively. On the other hand, the IL having the lower electrochemical stability was **$Pip_{1,8}$ (3)**.

Acknowledgements

Funding: This work was funded by Italy's Ministry of Education, University and Research (MIUR) under the Scientific funding program PRIN (Research Projects of Relevant National Interest). PRIN 2017Z8TS5B - "Tuning and understanding Quantum phases in 2D materials -Quantum2D".

References

[1] K. Ueno, H. Shimotani, H. Yuan, J. Ye, M. Kawasaki, Y. Iwasa, Field-Induced Superconductivity in Electric Double Layer Transistors, J. Phys. Soc. Japan. 83 (2014) 032001. https://doi.org/10.7566/JPSJ.83.032001.

[2] T. Fujimoto, K. Awaga, Electric-double-layer field-effect transistors with ionic liquids, Phys. Chem. Chem. Phys. 15 (2013) 8983. https://doi.org/10.1039/c3cp50755f.

[3] P. Liu, B. Lei, X. Chen, L. Wang, X. Wang, Superior carrier tuning in ultrathin superconducting materials by electric-field gating, Nat. Rev. Phys. 4 (2022) 336–352. https://doi.org/10.1038/s42254-022-00438-2.

[4] D. Daghero, F. Paolucci, A. Sola, M. Tortello, G.A. Ummarino, M. Agosto, R.S. Gonnelli, J.R. Nair, C. Gerbaldi, Large Conductance Modulation of Gold Thin Films by Huge Charge Injection via Electrochemical Gating, Phys. Rev. Lett. 108 (2012) 066807. https://doi.org/10.1103/PhysRevLett.108.066807.

[5] S. Shimizu, K.S. Takahashi, T. Hatano, M. Kawasaki, Y. Tokura, Y. Iwasa, Electrically Tunable Anomalous Hall Effect in Pt Thin Films, Phys. Rev. Lett. 111 (2013) 216803. https://doi.org/10.1103/PhysRevLett.111.216803.

[6] Y. Saito, Y. Iwasa, Ambipolar Insulator-to-Metal Transition in Black Phosphorus by Ionic-Liquid Gating, ACS Nano. 9 (2015) 3192–3198. https://doi.org/10.1021/acsnano.5b00497.

[7] D. Ovchinnikov, F. Gargiulo, A. Allain, D.J. Pasquier, D. Dumcenco, C.-H. Ho, O. V. Yazyev, A. Kis, Disorder engineering and conductivity dome in ReS2 with electrolyte gating, Nat. Commun. 7 (2016) 12391. https://doi.org/10.1038/ncomms12391.

[8] E. Piatti, F. Galanti, G. Pippione, A. Pasquarelli, R.S. Gonnelli, Towards the insulator-to-metal transition at the surface of ion-gated nanocrystalline diamond films, Eur. Phys. J. Spec. Top. 228 (2019) 689–696. https://doi.org/10.1140/epjst/e2019-800188-9.

[9] Y. Zhang, J. Ye, Y. Matsuhashi, Y. Iwasa, Ambipolar MoS 2 Thin Flake Transistors, Nano Lett. 12 (2012) 1136–1140. https://doi.org/10.1021/nl2021575.

[10] H. Yuan, H. Shimotani, A. Tsukazaki, A. Ohtomo, M. Kawasaki, Y. Iwasa, High-Density Carrier Accumulation in ZnO Field-Effect Transistors Gated by Electric Double Layers of Ionic Liquids, Adv. Funct. Mater. 19 (2009) 1046–1053. https://doi.org/10.1002/adfm.200801633.

[11] E. Piatti, D. Romanin, D. Daghero, R.S. Gonnelli, Two-dimensional hole transport in ion-gated diamond surfaces: A brief review (Review article), Low Temp. Phys. 45 (2019) 1143–1155. https://doi.org/10.1063/10.0000122.

[12] K. Ueno, S. Nakamura, H. Shimotani, A. Ohtomo, N. Kimura, T. Nojima, H. Aoki, Y. Iwasa, M. Kawasaki, Electric-field-induced superconductivity in an insulator, Nat. Mater. 7 (2008) 855–858. https://doi.org/10.1038/nmat2298.

[13] J.T. Ye, S. Inoue, K. Kobayashi, Y. Kasahara, H.T. Yuan, H. Shimotani, Y. Iwasa, Liquid-gated interface superconductivity on an atomically flat film, Nat. Mater. 9 (2010) 125–128. https://doi.org/10.1038/nmat2587.

[14] J.T. Ye, Y.J. Zhang, R. Akashi, M.S. Bahramy, R. Arita, Y. Iwasa, Superconducting Dome in a Gate-Tuned Band Insulator, Science (80-.). 338 (2012) 1193–1196. https://doi.org/10.1126/science.1228006.

[15] E. Piatti, Ionic gating in metallic superconductors: A brief review, Nano Express. 2 (2021) 024003. https://doi.org/10.1088/2632-959X/ac011d.

[16] W. Shi, J. Ye, Y. Zhang, R. Suzuki, M. Yoshida, J. Miyazaki, N. Inoue, Y. Saito, Y. Iwasa, Superconductivity Series in Transition Metal Dichalcogenides by Ionic Gating, Sci. Rep. 5 (2015) 12534. https://doi.org/10.1038/srep12534.

[17] L.J. Li, E.C.T. O'Farrell, K.P. Loh, G. Eda, B. Özyilmaz, A.H. Castro Neto, Controlling many-body states by the electric-field effect in a two-dimensional material, Nature. 529 (2016) 185–189. https://doi.org/10.1038/nature16175.

[18] X. Xi, H. Berger, L. Forró, J. Shan, K.F. Mak, Gate Tuning of Electronic Phase Transitions in Two-Dimensional NbSe2, Phys. Rev. Lett. 117 (2016) 106801. https://doi.org/10.1103/PhysRevLett.117.106801.

[19] B. Lei, J.H. Cui, Z.J. Xiang, C. Shang, N.Z. Wang, G.J. Ye, X.G. Luo, T. Wu, Z. Sun, X.H. Chen, Evolution of High-Temperature Superconductivity from a Low-Tc Phase Tuned by Carrier Concentration in FeSe Thin Flakes, Phys. Rev. Lett. 116 (2016) 077002. https://doi.org/10.1103/PhysRevLett.116.077002.

[20] E. Piatti, D. Daghero, G.A. Ummarino, F. Laviano, J.R. Nair, R. Cristiano, A. Casaburi, C. Portesi, A. Sola, R.S. Gonnelli, Control of bulk superconductivity in a BCS superconductor by surface charge doping via electrochemical gating, Phys. Rev. B. 95 (2017) 140501. https://doi.org/10.1103/PhysRevB.95.140501.

[21] J.G. Checkelsky, J. Ye, Y. Onose, Y. Iwasa, Y. Tokura, Dirac-fermion-mediated ferromagnetism in a topological insulator, Nat. Phys. 8 (2012) 729–733. https://doi.org/10.1038/nphys2388.

[22] S. Dushenko, M. Hokazono, K. Nakamura, Y. Ando, T. Shinjo, M. Shiraishi, Tunable inverse spin Hall effect in nanometer-thick platinum films by ionic gating, Nat. Commun. 9 (2018) 3118. https://doi.org/10.1038/s41467-018-05611-9.

[23] L. Liang, Q. Chen, J. Lu, W. Talsma, J. Shan, G.R. Blake, T.T.M. Palstra, J. Ye, Inducing ferromagnetism and Kondo effect in platinum by paramagnetic ionic gating, Sci. Adv. 4 (2018). https://doi.org/10.1126/sciadv.aar2030.

[24] I.A. Verzhbitskiy, H. Kurebayashi, H. Cheng, J. Zhou, S. Khan, Y.P. Feng, G. Eda, Controlling the magnetic anisotropy in Cr2Ge2Te6 by electrostatic gating, Nat. Electron. 3 (2020) 460–465. https://doi.org/10.1038/s41928-020-0427-7.

[25] Z. Wang, T. Zhang, M. Ding, B. Dong, Y. Li, M. Chen, X. Li, J. Huang, H. Wang, X. Zhao, Y. Li, D. Li, C. Jia, L. Sun, H. Guo, Y. Ye, D. Sun, Y. Chen, T. Yang, J. Zhang, S. Ono, Z. Han, Z. Zhang, Electric-field control of magnetism in a few-layered van der Waals ferromagnetic semiconductor, Nat. Nanotechnol. 13 (2018) 554–559. https://doi.org/10.1038/s41565-018-0186-z.

[26] J.H. Cho, J. Lee, Y. Xia, B. Kim, Y. He, M.J. Renn, T.P. Lodge, C. Daniel Frisbie, Printable ion-gel gate dielectrics for low-voltage polymer thin-film transistors on plastic, Nat. Mater. 7 (2008) 900–906. https://doi.org/10.1038/nmat2291.

[27] Y. Xia, W. Zhang, M. Ha, J.H. Cho, M.J. Renn, C.H. Kim, C.D. Frisbie, Printed Sub-2 V Gel-Electrolyte-Gated Polymer Transistors and Circuits, Adv. Funct. Mater. 20 (2010) 587–594. https://doi.org/10.1002/adfm.200901845.

[28] T. Fujimoto, Y. Miyoshi, M.M. Matsushita, K. Awaga, A complementary organic inverter of porphyrazine thin films: low-voltage operation using ionic liquid gate dielectrics, Chem. Commun. 47 (2011) 5837. https://doi.org/10.1039/c0cc05198e.

[29] M. Ha, Y. Xia, A.A. Green, W. Zhang, M.J. Renn, C.H. Kim, M.C. Hersam, C.D. Frisbie, Printed, Sub-3V Digital Circuits on Plastic from Aqueous Carbon Nanotube Inks, ACS Nano. 4 (2010) 4388–4395. https://doi.org/10.1021/nn100966s.

[30] H. Yuan, H. Shimotani, A. Tsukazaki, A. Ohtomo, M. Kawasaki, Y. Iwasa, Hydrogenation-Induced Surface Polarity Recognition and Proton Memory Behavior at Protic-Ionic-Liquid/Oxide Electric-Double-Layer Interfaces, J. Am. Chem. Soc. 132 (2010) 6672–6678. https://doi.org/10.1021/ja909110s.

[31] N.J. Kay, S.J. Higgins, J.O. Jeppesen, E. Leary, J. Lycoops, J. Ulstrup, R.J. Nichols, Single-Molecule Electrochemical Gating in Ionic Liquids, J. Am. Chem. Soc. 134 (2012) 16817–16826.

https://doi.org/10.1021/ja307407e.

[32] Y.J. Zhang, T. Oka, R. Suzuki, J.T. Ye, Y. Iwasa, Electrically Switchable Chiral Light-Emitting Transistor, Science (80-.). 344 (2014) 725–728. https://doi.org/10.1126/science.1251329.

[33] S.-K. Lee, S.M. Humayun Kabir, B.K. Sharma, B.J. Kim, J.H. Cho, J.-H. Ahn, Photo-patternable ion gel-gated graphene transistors and inverters on plastic, Nanotechnology. 25 (2014) 014002. https://doi.org/10.1088/0957-4484/25/1/014002.

[34] E. Piatti, A. Arbab, F. Galanti, T. Carey, L. Anzi, D. Spurling, A. Roy, A. Zhussupbekova, K.A. Patel, J.M. Kim, D. Daghero, R. Sordan, V. Nicolosi, R.S. Gonnelli, F. Torrisi, Charge transport mechanisms in inkjet-printed thin-film transistors based on two-dimensional materials, Nat. Electron. 4 (2021) 893–905. https://doi.org/10.1038/s41928-021-00684-9.

[35] S. Shimizu, J. Shiogai, N. Takemori, S. Sakai, H. Ikeda, R. Arita, T. Nojima, A. Tsukazaki, Y. Iwasa, Giant thermoelectric power factor in ultrathin FeSe superconductor, Nat. Commun. 10 (2019) 825. https://doi.org/10.1038/s41467-019-08784-z.

[36] P. Gallagher, M. Lee, T.A. Petach, S.W. Stanwyck, J.R. Williams, K. Watanabe, T. Taniguchi, D. Goldhaber-Gordon, A high-mobility electronic system at an electrolyte-gated oxide surface, Nat. Commun. 6 (2015) 6437. https://doi.org/10.1038/ncomms7437.

[37] E. Piatti, Q. Chen, M. Tortello, J. Ye, R.S. Gonnelli, Possible charge-density-wave signatures in the anomalous resistivity of Li-intercalated multilayer MoS2, Appl. Surf. Sci. 461 (2018) 269–275. https://doi.org/10.1016/j.apsusc.2018.05.232.

[38] H. Jo, J.-H. Choi, C.-M. Hyun, S.-Y. Seo, D.Y. Kim, C.-M. Kim, M.-J. Lee, J.-D. Kwon, H.-S. Moon, S.-H. Kwon, J.-H. Ahn, A Hybrid Gate Dielectrics of Ion Gel with Ultra-Thin Passivation Layer for High-Performance Transistors Based on Two-Dimensional Semiconductor Channels, Sci. Rep. 7 (2017) 14194. https://doi.org/10.1038/s41598-017-14649-6.

[39] E. Piatti, T. Hatano, D. Daghero, F. Galanti, C. Gerbaldi, S. Guastella, C. Portesi, I. Nakamura, R. Fujimoto, K. Iida, H. Ikuta, R.S. Gonnelli, Ambipolar suppression of superconductivity by ionic gating in optimally doped BaFe2(As,P)2 ultrathin films, Phys. Rev. Mater. 3 (2019) 044801. https://doi.org/10.1103/PhysRevMaterials.3.044801.

[40] E. Piatti, M. Colangelo, M. Bartoli, O. Medeiros, R.S. Gonnelli, K.K. Berggren, D. Daghero, Reversible tuning of superconductivity in ion-gated niobium nitride ultrathin films by self-encapsulation with a high-κ dielectric layer, (2022). http://arxiv.org/abs/2205.05491.

[41] J. Ye, M.F. Craciun, M. Koshino, S. Russo, S. Inoue, H. Yuan, H. Shimotani, A.F. Morpurgo, Y. Iwasa, Accessing the transport properties of graphene and its multilayers at high carrier density, Proc. Natl. Acad. Sci. 108 (2011) 13002–13006. https://doi.org/10.1073/pnas.1018388108.

[42] E. Uesugi, H. Goto, R. Eguchi, A. Fujiwara, Y. Kubozono, Electric double-layer capacitance between an ionic liquid and few-layer graphene, Sci. Rep. 3 (2013) 1595. https://doi.org/10.1038/srep01595.

[43] R.S. Gonnelli, F. Paolucci, E. Piatti, K. Sharda, A. Sola, M. Tortello, J.R. Nair, C. Gerbaldi, M. Bruna, S. Borini, Temperature Dependence of Electric Transport in Few-layer Graphene under Large Charge Doping Induced by Electrochemical Gating, Sci. Rep. 5 (2015) 9554. https://doi.org/10.1038/srep09554.

[44] R.S. Gonnelli, E. Piatti, A. Sola, M. Tortello, F. Dolcini, S. Galasso, J.R. Nair, C. Gerbaldi, E. Cappelluti, M. Bruna, A.C. Ferrari, Weak localization in electric-double-layer gated few-layer graphene, 2D Mater. 4 (2017) 035006. https://doi.org/10.1088/2053-1583/aa5afe.

[45] H. Zhang, C. Berthod, H. Berger, T. Giamarchi, A.F. Morpurgo, Band Filling and Cross Quantum Capacitance in Ion-Gated Semiconducting Transition Metal Dichalcogenide Monolayers, Nano Lett. 19 (2019) 8836–8845. https://doi.org/10.1021/acs.nanolett.9b03667.

[46] E. Piatti, A. Pasquarelli, R.S. Gonnelli, Orientation-dependent electric transport and band filling in hole co-doped epitaxial diamond films, Appl. Surf. Sci. 528 (2020) 146795. https://doi.org/10.1016/j.apsusc.2020.146795.

[47] C. Berthod, H. Zhang, A.F. Morpurgo, T. Giamarchi, Theory of cross quantum capacitance, Phys. Rev. Res. 3 (2021) 043036. https://doi.org/10.1103/PhysRevResearch.3.043036.

[48] S.K. Singh, A.W. Savoy, Ionic liquids synthesis and applications: An overview, J. Mol. Liq. 297 (2020)

112038. https://doi.org/10.1016/j.molliq.2019.112038.

[49] L.E. Shmukler, I.V. Fedorova, Y.A. Fadeeva, L.P. Safonova, The physicochemical properties and structure of alkylammonium protic ionic liquids of RnH4-nNX (n = 1–3) family. A mini–review, J. Mol. Liq. 321 (2021) 114350. https://doi.org/10.1016/j.molliq.2020.114350.

[50] B. Gaida, A. Brzęczek-Szafran, Insights into the Properties and Potential Applications of Renewable Carbohydrate-Based Ionic Liquids: A Review, Molecules. 25 (2020) 3285. https://doi.org/10.3390/molecules25143285.

[51] B. Likozar, The effect of ionic liquid type on the properties of hydrogenated nitrile elastomer/hydroxy-functionalized multi-walled carbon nanotube/ionic liquid composites, Soft Matter. 7 (2011) 970–977. https://doi.org/10.1039/C0SM00759E.

[52] B. Likozar, Diffusion of Ionic Liquids into Elastomer/Carbon Nanotubes Composites and Tensile Mechanical Properties of Resulting Materials, Sci. Iran. 17 (2010). http://scientiairanica.sharif.edu/article_3344.html.

[53] M. Grilc, B. Likozar, J. Levec, Kinetic model of homogeneous lignocellulosic biomass solvolysis in glycerol and imidazolium-based ionic liquids with subsequent heterogeneous hydrodeoxygenation over NiMo/Al2O3 catalyst, Catal. Today. 256 (2015) 302–314. https://doi.org/10.1016/j.cattod.2015.02.034.

[54] E. Husanu, A. Mero, J.G. Rivera, A. Mezzetta, J.C. Ruiz, F. D'Andrea, C.S. Pomelli, L. Guazzelli, Exploiting Deep Eutectic Solvents and Ionic Liquids for the Valorization of Chestnut Shell Waste, ACS Sustain. Chem. Eng. 8 (2020) 18386–18399. https://doi.org/10.1021/acssuschemeng.0c04945.

[55] M. Haque, I. Abdurrokhman, A. Idström, Q. Li, A. Rajaras, A. Martinelli, L. Evenäs, P. Lundgren, P. Enoksson, Exploiting low-grade waste heat to produce electricity through supercapacitor containing carbon electrodes and ionic liquid electrolytes, Electrochim. Acta. 403 (2022) 139640. https://doi.org/10.1016/j.electacta.2021.139640.

[56] O. Danyliv, M. Strach, O. Nechyporchuk, T. Nypelö, A. Martinelli, Self-Standing, Robust Membranes Made of Cellulose Nanocrystals (CNCs) and a Protic Ionic Liquid: Toward Sustainable Electrolytes for Fuel Cells, ACS Appl. Energy Mater. 4 (2021) 6474–6485. https://doi.org/10.1021/acsaem.1c00452.

[57] E. Jónsson, Ionic liquids as electrolytes for energy storage applications – A modelling perspective, Energy Storage Mater. 25 (2020) 827–835. https://doi.org/10.1016/j.ensm.2019.08.030.

[58] A. Triolo, V. Di Lisio, F. Lo Celso, G.B. Appetecchi, B. Fazio, P. Chater, A. Martinelli, F. Sciubba, O. Russina, Liquid Structure of a Water-in-Salt Electrolyte with a Remarkably Asymmetric Anion, J. Phys. Chem. B. 125 (2021) 12500–12517. https://doi.org/10.1021/acs.jpcb.1c06759.

[59] T. Welton, Ionic liquids: a brief history, Biophys. Rev. 10 (2018) 691–706. https://doi.org/10.1007/s12551-018-0419-2.

[60] A. Mezzetta, J. Łuczak, J. Woch, C. Chiappe, J. Nowicki, L. Guazzelli, Surface active fatty acid ILs: Influence of the hydrophobic tail and/or the imidazolium hydroxyl functionalization on aggregates formation, J. Mol. Liq. 289 (2019) 111155. https://doi.org/10.1016/j.molliq.2019.111155.

[61] A. Mero, A. Mezzetta, J. Nowicki, J. Łuczak, L. Guazzelli, Betaine and l-carnitine ester bromides: Synthesis and comparative study of their thermal behaviour and surface activity, J. Mol. Liq. 334 (2021) 115988. https://doi.org/10.1016/j.molliq.2021.115988.

[62] D.H. Zaitsau, N. Plechkova, S.P. Verevkin, Vaporization thermodynamics of ionic liquids with tetraalkylphosphonium cations, J. Chem. Thermodyn. 130 (2019) 204–212. https://doi.org/10.1016/j.jct.2018.10.007.

[63] L. Barulli, A. Mezzetta, B. Brunetti, L. Guazzelli, S. Vecchio Ciprioti, A. Ciccioli, Evaporation thermodynamics of the tetraoctylphosphonium bis(trifluoromethansulfonyl)imide([P8888]NTf2) and tetraoctylphosphonium nonafluorobutane-1-sulfonate ([P8888]NFBS) ionic liquids, J. Mol. Liq. 333 (2021) 115892. https://doi.org/10.1016/j.molliq.2021.115892.

[64] H.-J. Liaw, C.-C. Chen, Y.-C. Chen, J.-R. Chen, S.-K. Huang, S.-N. Liu, Relationship between flash point of ionic liquids and their thermal decomposition, Green Chem. 14 (2012) 2001. https://doi.org/10.1039/c2gc35449g.

[65] J. Noack, N. Roznyatovskaya, T. Herr, P. Fischer, The Chemistry of Redox- Flow Batteries, Angew. Chemie Int. Ed. 54 (2015) 9776–9809. https://doi.org/10.1002/anie.201410823.

[66] L. Guglielmero, M.M. Langroudi, M. Al Khatib, M.A.C. de Oliveira, B. Mecheri, M. De Leo, A. Mezzetta, L. Guazzelli, R. Giglioli, A. D'Epifanio, R. Pogni, C. Chiappe, C.S. Pomelli, Electrochemical and spectroscopic study of vanadyl acetylacetonate–ionic liquids interactions, Electrochim. Acta. 373 (2021) 137865. https://doi.org/10.1016/j.electacta.2021.137865.

[67] L. Guglielmero, A. Mero, A. Mezzetta, G. Tofani, F. D'Andrea, C.S. Pomelli, L. Guazzelli, Novel access to ionic liquids based on trivalent metal–EDTA complexes and their thermal and electrochemical characterization, J. Mol. Liq. 340 (2021) 117210. https://doi.org/10.1016/j.molliq.2021.117210.

[68] Q. Li, J. Jiang, G. Li, W. Zhao, X. Zhao, T. Mu, The electrochemical stability of ionic liquids and deep eutectic solvents, Sci. China Chem. 59 (2016) 571–577. https://doi.org/10.1007/s11426-016-5566-3.

[69] S.S. Moganty, R.E. Baltus, D. Roy, Electrochemical windows and impedance characteristics of [Bmim+][BF4-] and [Bdmim+][BF4-] ionic liquids at the surfaces of Au, Pt, Ta and glassy carbon electrodes, Chem. Phys. Lett. 483 (2009) 90–94. https://doi.org/10.1016/j.cplett.2009.10.063.

[70] P. Gancarz, E. Zorębski, M. Dzida, Influence of experimental conditions on the electrochemical window. Case study on bis(trifluoromethylsulfonyl)imide-based ionic liquids, Electrochem. Commun. 130 (2021) 107107. https://doi.org/10.1016/j.elecom.2021.107107.

[71] S. Doblinger, T.J. Donati, D.S. Silvester, Effect of Humidity and Impurities on the Electrochemical Window of Ionic Liquids and Its Implications for Electroanalysis, J. Phys. Chem. C. 124 (2020) 20309–20319. https://doi.org/10.1021/acs.jpcc.0c07012.

[72] M. Hayyan, F.S. Mjalli, M.A. Hashim, I.M. AlNashef, T.X. Mei, Investigating the electrochemical windows of ionic liquids, J. Ind. Eng. Chem. 19 (2013) 106–112. https://doi.org/10.1016/j.jiec.2012.07.011.

[73] C. Zhao, G. Burrell, A.A.J. Torriero, F. Separovic, N.F. Dunlop, D.R. MacFarlane, A.M. Bond, Electrochemistry of Room Temperature Protic Ionic Liquids, J. Phys. Chem. B. 112 (2008) 6923–6936. https://doi.org/10.1021/jp711804j.

[74] N. Sánchez-Ramírez, B.D. Assresahegn, D. Bélanger, R.M. Torresi, A Comparison among Viscosity, Density, Conductivity, and Electrochemical Windows of N - n -Butyl- N -methylpyrrolidinium and Triethyl- n - pentylphosphonium Bis(fluorosulfonyl imide) Ionic Liquids and Their Analogues Containing Bis(trifluoromethylsulfonyl), J. Chem. Eng. Data. 62 (2017) 3437–3444. https://doi.org/10.1021/acs.jced.7b00458.

[75] N. Lu, P. Zhang, Q. Zhang, R. Qiao, Q. He, H.-B. Li, Y. Wang, J. Guo, D. Zhang, Z. Duan, Z. Li, M. Wang, S. Yang, M. Yan, E. Arenholz, S. Zhou, W. Yang, L. Gu, C.-W. Nan, J. Wu, Y. Tokura, P. Yu, Electric-field control of tri-state phase transformation with a selective dual-ion switch, Nature. 546 (2017) 124–128. https://doi.org/10.1038/nature22389.

[76] A.R. Neale, S. Murphy, P. Goodrich, C. Hardacre, J. Jacquemin, Thermophysical and Electrochemical Properties of Ethereal Functionalised Cyclic Alkylammonium-based Ionic Liquids as Potential Electrolytes for Electrochemical Applications, ChemPhysChem. 18 (2017) 2040–2057. https://doi.org/10.1002/cphc.201700246.

[77] Z.-B. Zhou, H. Matsumoto, K. Tatsumi, Low-Melting, Low-Viscous, Hydrophobic Ionic Liquids: Aliphatic Quaternary Ammonium Salts with Perfluoroalkyltrifluoroborates, Chem. - A Eur. J. 11 (2005) 752–766. https://doi.org/10.1002/chem.200400817.

[78] M.L.P. Le, N.A. Tran, H.P.K. Ngo, T.G. Nguyen, V.M. Tran, Liquid Electrolytes Based on Ionic Liquids for Lithium-Ion Batteries, J. Solution Chem. 44 (2015) 2332–2343. https://doi.org/10.1007/s10953-015-0408-z.

[79] S.P. Ong, O. Andreussi, Y. Wu, N. Marzari, G. Ceder, Electrochemical Windows of Room-Temperature Ionic Liquids from Molecular Dynamics and Density Functional Theory Calculations, Chem. Mater. 23 (2011) 2979–2986. https://doi.org/10.1021/cm200679y.

[80] C. Lian, H. Liu, C. Li, J. Wu, Hunting ionic liquids with large electrochemical potential windows, AIChE J. 65 (2019) 804–810. https://doi.org/10.1002/aic.16467.

[81] W. Buijs, G.-J. Witkamp, M.C. Kroon, Correlation between Quantumchemically Calculated LUMO Energies and the Electrochemical Window of Ionic Liquids with Reduction-Resistant Anions, Int. J. Electrochem. 2012 (2012) 1–6. https://doi.org/10.1155/2012/589050.

[82] T. Takekiyo, Y. Imai, H. Abe, Y. Yoshimura, Conformational Analysis of Quaternary Ammonium-Type Ionic

Liquid Cation, N,N -Diethyl- N -methyl- N -(2-methoxyethyl) Ammonium Cation, Adv. Phys. Chem. 2012 (2012) 1–7. https://doi.org/10.1155/2012/829523.

[83] M.L.P. Le, F. Alloin, P. Strobel, J.-C. Leprêtre, C. Pérez del Valle, P. Judeinstein, Structure−Properties Relationships of Lithium Electrolytes Based on Ionic Liquid, J. Phys. Chem. B. 114 (2010) 894–903. https://doi.org/10.1021/jp9098842.

[84] M. Montanino, M. Carewska, F. Alessandrini, S. Passerini, G.B. Appetecchi, The role of the cation aliphatic side chain length in piperidinium bis(trifluoromethansulfonyl)imide ionic liquids, Electrochim. Acta. 57 (2011) 153–159. https://doi.org/10.1016/j.electacta.2011.03.089.

[85] G.B. Appetecchi, M. Montanino, M. Carewska, M. Moreno, F. Alessandrini, S. Passerini, Chemical–physical properties of bis(perfluoroalkylsulfonyl)imide-based ionic liquids, Electrochim. Acta. 56 (2011) 1300–1307. https://doi.org/10.1016/j.electacta.2010.10.023.

[86] Z.J. Chen, T. Xue, J.-M. Lee, What causes the low viscosity of ether-functionalized ionic liquids? Its dependence on the increase of free volume, RSC Adv. 2 (2012) 10564. https://doi.org/10.1039/c2ra21772d.

[87] T. Nokami, T. Yamashita, T. Komura, N. Handa, M. Shimizu, K. Yamaguchi, Y. Domi, H. Usui, H. Sakaguchi, T. Itoh, Effects of the ether oxygen atom in alkyl side chains on the physical properties of piperidinium ionic liquids, Faraday Discuss. 206 (2018) 523–534. https://doi.org/10.1039/C7FD00142H.

[88] A. Mezzetta, L. Guglielmero, A. Mero, G. Tofani, F. D'Andrea, C.S. Pomelli, L. Guazzelli, Expanding the Chemical Space of Benzimidazole Dicationic Ionic Liquids, Molecules. 26 (2021) 4211. https://doi.org/10.3390/molecules26144211.

[89] Z.-B. Zhou, H. Matsumoto, K. Tatsumi, Cyclic Quaternary Ammonium Ionic Liquids with Perfluoroalkyltrifluoroborates: Synthesis, Characterization, and Properties, Chem. - A Eur. J. 12 (2006) 2196–2212. https://doi.org/10.1002/chem.200500930.

[90] T. Song, O. Morales-Collazo, J.F. Brennecke, Solubility and Diffusivity of Oxygen in Ionic Liquids, J. Chem. Eng. Data. 64 (2019) 4956–4967. https://doi.org/10.1021/acs.jced.9b00750.

[91] F.F.C. Bazito, Y. Kawano, R.M. Torresi, Synthesis and characterization of two ionic liquids with emphasis on their chemical stability towards metallic lithium, Electrochim. Acta. 52 (2007) 6427–6437. https://doi.org/10.1016/j.electacta.2007.04.064.

[92] S. Men, P. Licence, C.-L. Do-Thanh, H. Luo, S. Dai, X-ray photoelectron spectroscopy of piperidinium ionic liquids: a comparison to the charge delocalised pyridinium analogues, Phys. Chem. Chem. Phys. 22 (2020) 11976–11983. https://doi.org/10.1039/D0CP01454K.

[93] C. Jagadeeswara Rao, K.A. Venkatesan, K. Nagarajan, T.G. Srinivasan, P.R. Vasudeva Rao, Electrochemical behavior of europium (III) in N-butyl-N-methylpyrrolidinium bis(trifluoromethylsulfonyl)imide, Electrochim. Acta. 54 (2009) 4718–4725. https://doi.org/10.1016/j.electacta.2009.03.074.

[94] S. Berdzinski, J. Horst, P. Straßburg, V. Strehmel, Recombination of Lophyl Radicals in Pyrrolidinium-Based Ionic Liquids, ChemPhysChem. 14 (2013) 1899–1908. https://doi.org/10.1002/cphc.201300098.

[95] T. Floris, P. Kluson, L. Bartek, H. Pelantova, Quaternary ammonium salts ionic liquids for immobilization of chiral Ru-BINAP complexes in asymmetric hydrogenation of β-ketoesters, Appl. Catal. A Gen. 366 (2009) 160–165. https://doi.org/10.1016/j.apcata.2009.07.002.

[96] Z. Chen, S. Liu, Z. Li, Q. Zhang, Y. Deng, Dialkoxy functionalized quaternary ammonium ionic liquids as potential electrolytes and cellulose solvents, New J. Chem. 35 (2011) 1596. https://doi.org/10.1039/c1nj20062c.

[97] Y. Yoshida, G. Saito, Ionic liquids based on diethylmethyl(2-methoxyethyl)ammonium cations and bis(perfluoroalkanesulfonyl)amide anions: influence of anion structure on liquid properties, Phys. Chem. Chem. Phys. 13 (2011) 20302. https://doi.org/10.1039/c1cp21783f.

[98] H. NOBUAKI, YAMADA YOSHIMI, QUATERNARY AMMONIUM SALTS, EP1595863B1, 2010.

[99] T. Nokami, K. Matsumoto, T. Itoh, Y. Fukaya, T. Itoh, Synthesis of Ionic Liquids Equipped with 2-Methoxyethoxymethyl/Methoxymethyl Groups Using a Simple Microreactor System, Org. Process Res. Dev. 18 (2014) 1367–1371. https://doi.org/10.1021/op500131u.

[100] R. Kawai, S. Yada, T. Yoshimura, Characterization and Solution Properties of Quaternary-Ammonium-Salt-Type Amphiphilic Gemini Ionic Liquids, ACS Omega. 4 (2019) 14242–14250.

https://doi.org/10.1021/acsomega.9b01660.

[101] S. Giri, R. Inostroza-Rivera, B. Herrera, A.S. Núñez, F. Lund, A. Toro-Labbé, The mechanism of Menshutkin reaction in gas and solvent phases from the perspective of reaction electronic flux, J. Mol. Model. 20 (2014) 2353. https://doi.org/10.1007/s00894-014-2353-y.

[102] A. Mezzetta, V. Perillo, L. Guazzelli, C. Chiappe, Thermal behavior analysis as a valuable tool for comparing ionic liquids of different classes, J. Therm. Anal. Calorim. 138 (2019) 3335–3345. https://doi.org/10.1007/s10973-019-08951-w.

[103] E. Gómez, N. Calvar, Á. Domínguez, E.A. Macedo, Thermal behavior and heat capacities of pyrrolidinium-based ionic liquids by DSC, Fluid Phase Equilib. 470 (2018) 51–59. https://doi.org/10.1016/j.fluid.2018.04.003.

[104] A. Triolo, O. Russina, B. Fazio, G.B. Appetecchi, M. Carewska, S. Passerini, Nanoscale organization in piperidinium-based room temperature ionic liquids, J. Chem. Phys. 130 (2009) 164521. https://doi.org/10.1063/1.3119977.

[105] G.B. Appetecchi, M. Montanino, D. Zane, M. Carewska, F. Alessandrini, S. Passerini, Effect of the alkyl group on the synthesis and the electrochemical properties of N-alkyl-N-methyl-pyrrolidinium bis(trifluoromethanesulfonyl)imide ionic liquids, Electrochim. Acta. 54 (2009) 1325–1332. https://doi.org/10.1016/j.electacta.2008.09.011.

[106] H. Shirota, H. Fukazawa, T. Fujisawa, J.F. Wishart, Heavy Atom Substitution Effects in Non-Aromatic Ionic Liquids: Ultrafast Dynamics and Physical Properties, J. Phys. Chem. B. 114 (2010) 9400–9412. https://doi.org/10.1021/jp1021104.

[107] L.T.M. Le, T.D. Vo, K.H.P. Ngo, S. Okada, F. Alloin, A. Garg, P.M.L. Le, Mixing ionic liquids and ethylene carbonate as safe electrolytes for lithium-ion batteries, J. Mol. Liq. 271 (2018) 769–777. https://doi.org/10.1016/j.molliq.2018.09.068.

[108] A. Gumyusenge, D.T. Tran, X. Luo, G.M. Pitch, Y. Zhao, K.A. Jenkins, T.J. Dunn, A.L. Ayzner, B.M. Savoie, J. Mei, Semiconducting polymer blends that exhibit stable charge transport at high temperatures, Science (80-.). 362 (2018) 1131–1134. https://doi.org/10.1126/science.aau0759.

[109] J. Reiter, E. Paillard, L. Grande, M. Winter, S. Passerini, Physicochemical properties of N-methoxyethyl-N-methylpyrrolidinum ionic liquids with perfluorinated anions, Electrochim. Acta. 91 (2013) 101–107. https://doi.org/10.1016/j.electacta.2012.12.086.

[110] I. Gualandi, M. Tessarolo, F. Mariani, D. Arcangeli, L. Possanzini, D. Tonelli, B. Fraboni, E. Scavetta, Layered Double Hydroxide-Modified Organic Electrochemical Transistor for Glucose and Lactate Biosensing, Sensors. 20 (2020) 3453. https://doi.org/10.3390/s20123453.

[111] P. Vanýsek, Impact of electrode geometry, depth of immersion, and size on impedance measurements, Can. J. Chem. 75 (1997) 1635–1642. https://doi.org/10.1139/v97-194.

[112] M. Vafaiee, M. Vossoughi, R. Mohammadpour, P. Sasanpour, Gold-Plated Electrode with High Scratch Strength for Electrophysiological Recordings, Sci. Rep. 9 (2019) 2985. https://doi.org/10.1038/s41598-019-39138-w.